An improved closed-form solution to interfacial stresses in plated beams using a two-stage approach

Jian Yang[*1] and Jianqiao Ye[2]

[1]*School of Civil Engineering, University of Birmingham, Edgbaston, Birmingham, B15 2TT, UK*

[2]*School of Civil Engineering, The University of Leeds, LS2 9JT, UK*

Abstract

The shear stress and the normal stresses in the thickness direction at interfaces (referred as interfacial shear and transverse normal stresses hereafter) have played a significant role in understanding the premature debonding failure of beams strengthened by bonding steel/composite plates at their tension surfaces. Due to the occurrence of dissimilar materials and the abrupt change of the cross section, the stress distribution at plate ends becomes singular and hence is considerably complicated. Extensive experimental and analytical analyses have been undertaken to investigate this problem. Large discrepancies have been found from various studies, particularly from experimental results due to the well-acknowledged difficulty in measuring interfacial stresses. Numerical analyses, e.g. 2-D or 3-D finite element analysis (FEA), may predict accurate results, but they demand laborious work on meshing and sensitivity analysis. Analytical solutions, in particular those in a closed form, are more desirable by engineering practitioners, as they can be readily incorporated into design equations. This paper reports an improved closed-form solution to interfacial stresses in plated beams using a two-stage approach. In this solution, beams and bonded plates can be further divided into a number of sub-layers to facilitate the inclusion of steel bars or multiple laminae. Thermal effects may also be considered by using equivalent mechanical loads, i.e. equivalent axial loads and end moments. Numerical examples are presented to show interfacial stresses in concrete or

* Corresponding author. Tel: +44 121 4145149; fax: +44 121 4143675

E-mail address: j.yang.3@bham.ac.uk

cast iron beams bonded with steel or FRP plates under mechanical and/or thermal loads. The effect of including the steel reinforcement with various ratios in the RC beam on the interfacial stresses is also investigated. Compared with previously published analytical results, this one improves the accuracy of predicting the transverse normal stresses in both adhesive-beam and plate-adhesive interfaces and the solution is in a closed form.

Keywords: FRP, reinforced concrete beams, cast iron beams, strengthening, interfacial stresses, stress concentration, debonding failure, thermal-mechanical loads.

Nomenclature

A, B	intermediate parameters defined in Equations A3.1-2
A_0	cross sectional area transformed to the first sub-layer of the plate
$A_0^{[i]}$	equivalent cross sectional area of the i –th layer transformed into the 1st sub-layer
a_m , b_m	Fourier coefficients
b	width of the adhesive layer
$b^{(i)}$	breadth of the i-th interface
$b^{[i,j]}$	width of the j-th sub-layer of the i-th layer
C_1,C_2,C_3	constants defined in Equation 17
$E_x^{[i,j]}$	Young's modulus in the j-th sub-layer of the i-th layer in the x-direction
$E_y^{[2]}$	Young's modulus in the adhesive layer in the y-direction
F_i	coefficients defined in Equation A3.3-7
$G_{xy}^{[2]}$	shear modulus of the adhesive layer
G_{1I},G_{2R},G_{2I}, G'_1,G'_2	functions defined in Equations 25a-e
$h^{[i]}$	height of the i-th layer
$h^{(i,j)}$	local y-coordinate of the j-th interface of the i-th layer
$h_0^{[i]}$	height of the centroid of the plate (i = 1) or the beam (i = 3)
I	square root of -1
I_0	second moment of area of the entire cross section transformed to the

	material of the first sub-layer of the plate defined in Equation A1.2
$I_0^{[i]}$	equivalent second moment of area of the *i*–th layer transformed into the 1st sub-layer
$h^{[i]}$	thickness of the *i*-th layer
H_i	intermediate parameters
L	half span length of the beam
l	half length of the bonded plate
M_0	applied bending moment
M_l	internal bending moment experienced in the cross section at the plate end
$M^{[i]}(x)$	internal bending moment in the *i*-th layer
N_0	applied axial force
N_i	number of sub-layers in the *i*-th layer
N_l	internal axial force experienced by the cross section at the plate end
$N^{[i]}(x)$	internal axial force in the *i*-th layer
P_m	loading coefficient defined in Equation 13d
P_m'	loading coefficient defined in Equation 21c
q	intensity of the uniformly distributed load
Q_l	internal shear force experienced by the cross section at the plate end
R	intermediate parameter defined in Equation 15c
R'	constant defined in Equation A3.18-29
$S_1,\ S_2,\ S_3$	intermediate parameters defined in Equations 13a-c
$S_1',\ S_2'$	intermediate parameters defined in Equations 21a-b
U	complementary energy
α	$=\sqrt{S_1 l^2 / 2S_3\pi^2}$
α'	$=\sqrt{S_1' l^2 / 2S_2'\pi^2}$
β	$=S_2 l^2 / 2S_3\pi^2$
$\delta_{11}, \delta_{12},$ δ_{21}, δ_{22}	constants defined in Equations 25f-i

γ_1 $= \sqrt{\beta + \sqrt{\beta^2 - \alpha^2}}$

γ_2 $= \sqrt{\beta - \sqrt{\beta^2 - \alpha^2}}$

η $= \sqrt{\alpha'/2}$

$\sigma_{xa}^{[i,j]}, \sigma_{xb}^{[i,j]}$ stress components defined in Equations 19c-e

$\sigma_{xy}^{[2]}(x)$ shear stresses in the adhesive layer

$\sigma_y^{(i)}(x)$ transverse normal stresses at the *i*-th interface

$\sigma_y^{[2]}(x)$ transverse normal stresses in the adhesive layer

$\sigma_{y0}(x)$ transverse normal stresses in the MA section of the adhesive layer

ξ $= a_m l / b_m m\pi$

$\Theta, \overline{\Theta}$ constants derived in Appendix II

$[i,j]$ The *j*-the sub-layer in the *i*-th layer (*i* =1 for the plate, *i* =3 for the beam)

1. Introduction

Reinforced concrete (RC) beams or metallic beams can be strengthened by bonding steel or composite plates/sheets to tension surfaces [1, 2]. Numerous studies have shown that this method improves their structural behaviours efficiently [3, 4]. However, a key problem arising in this application is the premature debonding failure, i.e. bonded plates separate from original beams and hence strengthened systems lose their integrity. The load at which the debonding failure occurs is much lower than the ultimate load resulting from the full composite action and hence usually becomes the governing design load for strengthened beams. As has been well acknowledged, the debonding failure is closely related to the high interfacial stresses near plate ends. Hence, a reliable prediction of interfacial stresses is prerequisite. Due to the occurrence of dissimilar materials and the abrupt change of the cross section, stresses at plate ends become singular and the prediction is considerably complicated. Extensive experimental [5-7] and analytical analyses [8-22] have been undertaken to investigate interfacial stresses for plated beams. Smith and Teng [8] and Mukhopadhyaya and Swamy [23] have compared various analytical solutions available. A more thorough and recent review has been done by Yang

[24], in which published experimental, numerical and analytical investigations have been reviewed. Large discrepancies have been found from various studies, particularly from experimental results due to the well-acknowledged difficulty in measuring interfacial stresses. Numerical analyses, e.g. 2-D and 3-D finite element analysis (FEA), may predict more rigorous results than analytical methods because less simplified assumptions are adopted in the modelling process, but they demand tedious work on meshing and convergence analysis. Analytical solutions, particularly, of the closed form, are desirable in engineering practice. Most analytical work is based on the assumption that shear and transverse normal stresses are uniform across the thickness of the adhesive layer [8-19]. The obtained solutions also violate the traction-free boundary condition at ends of the adhesive layer. Shen et al. [20] proposed a closed-form high-order solution for the strengthened beam subjected to uniformly distributed load (UDL), where the adhesive layer was treated as a 2-D medium. Yang et al. [21] extended it to arbitrary loading conditions. The predicted shear stresses from these solutions agreed well with FEA results except for transverse normal stresses. None of the above closed-form solutions have taken into account the effect of steel reinforcements in RC beams, and the application of high-order solutions were only limited to rectangular solid cross sections.

This paper reports an improved closed-form solution to interfacial stresses in plated beams using a two-stage approach. Unlike FEA method, this solution can avoid the cumbersome work of meshing and convergence analysis. Hence it can be particularly useful in performing extensive parametric analysis. As an explicit solution, the result can be obtained without computer coding requirement. A spreadsheet package such as MS Excel will be sufficient. Compared with other analytical solutions, one of the major improvements of this solution is that it can accurately predict the transverse normal stresses in both adhesive-beam (AB) and plate-adhesive (PA) interfaces. Stress solutions satisfy the traction-free boundary condition. By introducing the concept of sublayers, this solution can also be utilised for beams and bonded plates with generic cross sections and multilayer materials. Although the solutions are derived for mechanical loads, thermal effects can also be included by employing the equivalent mechanical loads.

Compared with the high-order solution by Rabinovich and Frostig [22], the present solution essentially offers the same level of accuracy. However, Rabinovich and Frostig's solution is not effectively a closed-form solution, where there are eleven integration constants that have to be calculated numerically. Special computer packages, such as Maple, have to be used to avoid numeric overflow problems. These problems do not exist in the present solution.

2. Method of solutions

2.1. Structural idealization of the strengthened beam

We consider a simply supported beam subjected to a uniformly distributed load (UDL) q, a pair of equal end forces N_0 and symmetric end moments M_0. The beam has a span length $2L$ and may have an arbitrary cross-sectional shape. It is partially strengthened by externally bonding a plate/sheet using structural adhesive, e.g. epoxy resin. The length of the bonded zone is $2l$. The structural idealization of the beam and applied loads are illustrated in Figure 1. The end axial force N_0 is assumed to be exerted through the centroid of the beam cross section. Under applied loads, internal forces including axial and shear forces and bending moment, denoted by $N_{l,,}$ Q_l and M_l respectively, are induced in the cross-sections of the bonded beam at plate ends. The sign convention for applied loads and internal forces is shown in Figure 2. A global Cartesian co-ordinate system x-y is used with its origin locating in the middle of the top surface of the beam (Figure 2a). The beam and the plate may be divided into a number of layers to facilitate the inclusion of various material properties and/or widths. In the case of the homogenous material with the constant width, only one layer is required. In the bonded zone, the beam consists of three major layers: the original beam, the adhesive layer and the plate. A local coordinate system $x^{[i]}$ - $y^{[i]}$ is adopted for each of them, with the origin being at the centroid of each layer (Figure 2a). The notations associated with each layer use the layer number as superscripts (e.g. the thicknesses of three layers are denoted by $h^{[1]}$, $h^{[2]}$ and $h^{[3]}$ respectively). Similarly, superscripts $^{(0)}$, $^{(1)}$, $^{(2)}$ and $^{(3)}$ are used to denote the surfaces and interfaces (e.g. the interfacial transverse normal stresses are denoted by $\sigma_y^{(1)}$ and $\sigma_y^{(2)}$). Each layer can be further divided into sub-layers, which are made of homogeneous or

equivalent homogeneous material and have a uniform width. The number of sub-layers depends on the composition of the cross sections. For instance, an I-beam can be divided into three layers with different widths, while a reinforced rectangular concrete beam can also be divided into three layers, one of which is the strip of concrete containing rebars. If a composite laminate is bonded to the beam, each lamina is a sub-layer. The adhesive layer, usually made from isotropic material, contains only one sub-layer and the width is denoted by *b* [Figure 2 (b)]. Figure 2 (c) shows detailed notations for labelling each sub-layer, e.g. the double superscripts $^{[3,\,i]}$ denotes the *i*-th sub-layer of the beam.

2.2. The rationale and the description of the method

Previous studies on RC beams, e.g. Shen et al. [20] and Yang et al. [21], revealed that the shear stresses at AB and PA interfaces are very close to each other. This observation is adopted in the present method, i.e. a uniform shear stress distribution is assumed over the thickness of the adhesive layer. In fact, this assumption implies that the adhesive layer does not carry any longitudinal normal stress, which is rational due to the fact that the Young's modulus of the adhesive layer is much lower than those of adherends. FEA modelling, e.g., Yang [24] and Teng et al. [25], have shown a significant variation in transverse normal stress across the adhesive thickness. It changes from the tension at the AB interface to the compression at the PA interface near plate ends. One of the objectives of this solution is to capture this variation.

In the present study, interfacial stresses are derived in two stages. In both stages, Fourier series are used to represent stresses and the principle of the complementary energy is applied. An explicit form of the infinite sum of Fourier series can be derived to represent stresses, thus leading to a closed-form solution. In the first stage, distributions of the shear and the normal stresses along the middle section of the adhesive layer are assumed and the relationship between these two is introduced based on the assumption of the composite action, therefore reducing the number of the unknown coefficients. However, in this stage, the resulting transverse normal stress can not achieve satisfactory accuracy due to this imposed relationship. To improve this, in the second stage, this imposed constraint is relaxed. Other stress components are represented in terms of the obtained

interfacial shear stress and applied loads. In both stages, equilibrium conditions will be satisfied *a priori* and the compatibility condition of stress components will be satisfied by implementing the principle of the complementary energy.

In developing the formulation, the following assumptions are adopted:

(a) Each individual sub-layer is elastic, homogeneous, although the major layers may be heterogeneous, e.g. bonded laminates and RC beams containing reinforcement.

(b) The layers/sub-layers are perfectly bonded (no slips or opening-up at the interfaces);

(c) Plane sections remain plane in the plate and the beam, respectively;

(d) The adhesive layer is considered to be in a plane stress state;

(e) The shear stress in the adhesive layer is uniform over the thickness;

(f) Stress distributions in width direction are uniform;

(g) In the first stage, the assumption of composite behaviour is used to define the relationship between the transverse normal stress and the shear stress along the middle section of the adhesive layer.

2.3. Equilibrium equations

In the beam (i =3) and the plate (i = 1), equilibriums of the axial force and the bending moment lead to the following equations :

$$\frac{dN^{[i]}(x)}{dx} = b^{(i)}\sigma_{xy}^{(i)}(x) - b^{(i-1)}\sigma_{xy}^{(i-1)}(x) \qquad (i = 1 \text{ or } 3) \tag{1a}$$

$$\frac{dM^{[i]}(x)}{dx} = Q^{[i]}(x) - \frac{h^{[i]}}{2}\left[b^{(i-1)}\sigma_{xy}^{(i-1)}(x) + b^{(i)}\sigma_{xy}^{(i)}(x)\right] \qquad (i = 1 \text{ or } 3) \tag{1b}$$

where $N^{[i]}(x)$ and $M^{[i]}(x)$ are the respective axial force and bending moment in the i^{th} layer and $\sigma_{xy}^{(i)}(x)$ and $\sigma_{y}^{(i)}(x)$ are the shear and transverse normal stresses at the i^{th} interface, e.g. i =1 for the PA interface and i = 3 for the AB interface. In Equations 1a and 1b and the rest of this paper, the superscript in $x^{[i]}$ is omitted because the global and the three local co-ordinate systems share the same horizontal axis.

The force boundary conditions at the ends of the plate are

$$N^{[i]}(\pm l) = \begin{cases} 0 & (i=1) \\ N_l & (i=3) \end{cases} \tag{2a}$$

$$M^{[i]}(\pm l) = \begin{cases} 0 & (i=1) \\ M_l & (i=3) \end{cases} \tag{2b}$$

According to assumption (d), equilibrium equations of the adhesive layer in the local coordinate system are

$$\frac{\partial \sigma_x^{[2]}}{\partial x} + \frac{\partial \sigma_{xy}^{[2]}}{\partial y^{[2]}} = 0 \tag{3a}$$

$$\frac{\partial \sigma_{xy}^{[2]}}{\partial x} + \frac{\partial \sigma_y^{[2]}}{\partial y^{[2]}} = 0 \tag{3b}$$

where $\sigma_x^{[2]}$, $\sigma_{xy}^{[2]}$ and $\sigma_y^{[2]}$ denote the longitudinal, shear and transverse normal stresses respectively; and $y^{[2]}$ is the local transverse coordinate for the adhesive layer.

2.4. Stage I: shear stress in the adhesive layer

The shear stress in the adhesive layer $\sigma_{xy}^{[2]}$ is constant by following assumption (e), which leads to a zero axial stress. Introducing the transverse normal stress in the MA section, denoted by σ_{y0}, and integrating Equation (3b) about $y^{[2]}$, the transverse normal stress in the adhesive layer $\sigma_y^{[2]}$ can be calculated by

$$\sigma_y^{[2]} = \sigma_{y0} - y^{[2]} \frac{d\sigma_{xy}^{[2]}}{dx} \tag{4}$$

Apparently, $\sigma_{xy}^{[2]}$ and σ_{y0} are functions of the *x* coordinate.

According to the antisymmetry and the symmetry nature of the shear and the normal stresses, $\sigma_{xy}^{[2]}$ and σ_{y0} may be expanded into Fourier series as follows,

$$\sigma_{xy}^{[2]}(x) = \sum_m b_m \sin\frac{m\pi x}{l} \; ; \qquad \sigma_{y0}(x) = \sum_m a_m \cos\frac{m\pi x}{l} \tag{5a, b}$$

where a_m and b_m are unknown Fourier coefficients; and m = 1, 2, …∞. Note that the constant term in Equation 5b has been set to zero to satisfy the equilibrium requirement that the integration of the interfacial normal stress over the entire length of the middle

section must be equal to zero. To facilitate the derivation of the closed-form solution, we introduce a coefficient ξ defined as follows

$$\xi = \frac{a_m}{b_m}\frac{l}{m\pi} \tag{6}$$

which is derived in Appendix I.

The substitution of Equations 5a and b and Equation 6 into Equation 4 leads to

$$\sigma_y^{[2]} = \left(-y^{[2]}\right)\sum_m b_m \frac{m\pi}{l}\cos\frac{m\pi x}{l} \tag{7}$$

Solving the force equilibrium and boundary conditions in Equations 1 and 2 and substituting Equations 5 and 6, we obtain

$$N^{[i]}(x) = b\sum_m \left(\frac{l}{m\pi}\right) b_m \left[\left(-1\right)^m - \cos\frac{m\pi x}{l}\right] + \begin{cases} 0 & i=1 \\ N_l & i=3 \end{cases} \tag{8a}$$

$$M^{[i]}(x) = -b\left\{\sum_m \left(\frac{l}{m\pi}\right) b_m \left[\left(-1\right)^m - \cos\frac{m\pi x}{l}\right]\right\} + \begin{cases} \left(\dfrac{2h^{[1]} - 2h_0^{[1]} - 2\xi + h^{[2]}}{2}\right) & i=1 \\ \left(h^{[2]} + 2h_0^{[3]} + 2\xi\right) + M_l + \dfrac{q\left(l^2 - x^2\right)}{2} & i=3 \end{cases} \tag{8b}$$

where $h_0^{[i]}$ is the height of the centroid of the plate (i =1) or the beam (i =3) (see Figure 2b).

By following assumption (c) where strains are linearly distributed along the beam and the plate, axial stress in the j-th sub-layer of the beam and the bonded plate can be obtained by transforming their cross sections into the equivalent ones made of the first sub-layer material and is given as follows:

$$\sigma_x^{[i,j]} = \frac{E_x^{[i,j]}}{E_x^{[i,1]}}\left(\frac{N^{[i]}}{A_0^{[i]}} + \frac{y^{[i]}M^{[i]}}{I_0^{[i]}}\right) \qquad (i = 1 \text{ and } 3) \tag{9}$$

where $E_x^{[i,j]}$ is the Young's modulus in the x-direction for the j-th sub-layer; $A_0^{[i]}$ and $I_0^{[i]}$ are, respectively, the equivalent cross sectional area and the second moment of area of the

cross section that has been transformed to the material of the 1st sub-layer. $y^{[i]}$ is the local transverse coordinate. The substitution of Equations 8a and 8b into Equation 9 leads to

$$\sigma_x^{[1,j]} = b\frac{E_x^{[1,j]}}{E_x^{[1,1]}}\left\{\frac{1}{A_0^{[1]}} - \frac{y^{[1]}}{2I_0^{[1]}}\left[h^{[1]} - 2h_0^{[1]} - 2\xi + h^{[2]}\right]\right\}\sum_m \frac{l}{m\pi} b_m\left[(-1)^m - \cos\frac{m\pi x}{l}\right]$$

$$\sigma_x^{[3,j]} = b\frac{E_x^{[3,j]}}{E_x^{[3,1]}}\left\{-\frac{1}{A_0^{[3]}} - \frac{y^{[3]}}{2I_0^{[3]}}\left[h^{[2]} + 2h_0^{[3]} + 2\xi\right]\right\}\sum_m \frac{l}{m\pi} b_m\left[(-1)^m - \cos\frac{m\pi x}{l}\right] + \frac{E_x^{[3,i]}}{E_x^{[3,1]}}\left\{\frac{N_0}{A_0^{[3]}} + \frac{y^{[3]}}{I_0^{[3]}}\left[M_l + \frac{q(l^2 - x^2)}{2}\right]\right\}$$

(10a, b)

The shear and transverse normal stress are assumed to be zero in the beam and the plate as it is believed that the interfacial stresses are mainly caused by the mismatch of axial stresses in these two adherends.

The unknown coefficients can be determined by the implementation of the principle of complementary energy in the strengthened beam. Only half of the beam is considered here owing to the symmetry of the structure and the loading, of which the complementary energy is

$$U = \frac{1}{2}\int_{-h^{[i]}/2}^{h^{[i]}/2}\int_0^l \left[\frac{1}{E_y^{[2]}}(\sigma_y^{[2]})^2 + \frac{1}{G_{xy}^{[2]}}(\tau_{xy}^{[2]})^2\right]dxdy^{[i]} + \frac{1}{2}\sum_{i=1,3}\sum_{j=1}^{N_i} b^{[i,j]}\frac{E_x^{[i,j]}}{(E_x^{[i,1]})^2}\int_{-h^{[i]}/2}^{h^{[i]}/2}\int_0^l (\sigma_x^{[i.j]})^2 dxdy^{[i]} \tag{11}$$

where $E_y^{[2]}$, $G_{xy}^{[2]}$ and $\nu_{xy}^{[2]}$ are the Young's moduli in the *y*-directions, the shear modulus and Poisson's ratio in the *x*-*y* plane of the adhesive layer, respectively; N_i is the number of sub-layers in the *i*-th layer.

Substituting the stress components in Equations 5a, 7, 10a and b into Equation 11 and minimising the complementary energy by equating the first-order differentiation with respect to b_m to zero yield

$$S_1\left(\frac{l}{m\pi}\right)(-1)^m \sum_{j=1,2,\cdots}\left(\frac{l}{j\pi}\right) b_j (-1)^j + \left[\frac{S_1}{2}\left(\frac{l}{m\pi}\right)^2 + S_2 + S_3\left(\frac{m\pi}{l}\right)^2\right] b_m = P_m \tag{12}$$

where

$$S_1 = \sum_{j=1}^{N_1} \frac{2b^{[1,j]}E_x^{[1,j]}I_0^{[1]}}{3(E_x^{[1,1]})^2(h_0^{[1]} + 2\xi - 2h^{[1]} - h^{[2]})}\left\{\left[\frac{1}{A_0^{[1]}} + \frac{h^{(1,j)}}{2I_0^{[1]}}(h_0^{[1]} + 2\xi - 2h^{[1]} - h^{[2]})\right]^3 - \left[\frac{1}{A_0^{[1]}} + \frac{h^{(1,j-1)}}{2I_0^{[1]}}(h_0^{[1]} + 2\xi - 2h^{[1]} - h^{[2]})\right]^3\right\}$$

$$-\sum_{j=1}^{N_3}\frac{2b^{[1,j]}E_x^{[3,j]}I_0^{[3]}}{3\left(E_x^{[3,1]}\right)\left(h_0^{[3]}+2\xi+h^{[2]}\right)}\left\{\left[\frac{1}{A_0^{[3]}}+\frac{h^{(1,j)}}{2I_0^{[3]}}\left(h_0^{[3]}+2\xi+h^{[2]}\right)\right]^3-\left[\frac{1}{A_0^{[3]}}+\frac{h^{(1,j-1)}}{2I_0^{[3]}}\left(h_0^{[3]}+2\xi+h^{[2]}\right)\right]^3\right\} \tag{13a}$$

$$S_2=\frac{h^{[2]}b}{2G_{xy}^{[2]}} \tag{13b}$$

$$S_3=\frac{bh^{[2]}}{24E_y^{[2]}}\left[\left(h^{[2]}\right)^2+12\xi^2\right] \tag{13c}$$

$$P_m=A\frac{\left(-1\right)^m}{m}+B\frac{\left(-1\right)^m}{m^3} \tag{13d}$$

In the above equations, $h^{(i,j)}$ is the local *y* coordinate of the *j*-th interface of the plate (*i* = 1) and the beam (*i* = 3) and therefore $h^{(i,0)}$ and $h^{(i,N_i)}$ are for the bottom and top surfaces, respectively. The coefficients A and B are listed in Appendix III.

Rewriting Equation 12 yields

$$b_m=\frac{m^4}{m^4+2\beta m^2+\alpha^2}\left[P_m-\left(\frac{l}{m\pi}\right)\left(-1\right)^m RS_1\right]\frac{1}{S_3} \tag{14}$$

where

$$\beta=\left(\frac{l}{\pi}\right)^2\frac{S_2}{2S_3};\ \alpha=\left(\frac{l}{\pi}\right)^2\sqrt{\frac{S_1}{2S_3}};\ R=\frac{l^2\pi^2\bar{\Theta}}{\pi^4S_3+l^4S_1\Theta};$$

$$\Theta=\sum_m\frac{1}{m^4+2\beta m^2+\alpha^2};\ \bar{\Theta}=\sum_m\frac{-1^{\ m}mP_m}{m^4+2\beta m^2+\alpha^2} \tag{15a-e}$$

The infinite sum of series Θ and $\bar{\Theta}$ are constants and they are derived in Appendix II.

Substitute Equations 14 and 15 into Equation 5a yields

$$\sigma_{xy}^{[2]}=\frac{l^2}{\pi^2S_3}\left\{\left(A-\frac{lS_1R}{\pi}\right)\sum_m\frac{\left(-1\right)^m m}{m^4+2\beta m^2+\alpha^2}\sin\left(\frac{m\pi}{l}x\right)+B\sum_m\frac{\left(-1\right)^m}{m\left(m^4+2\beta m^2+\alpha^2\right)}\sin\left(\frac{m\pi}{l}x\right)\right\}$$
$$=C_1\sinh\left(\frac{\gamma_1\pi}{l}x\right)+C_2\sinh\left(\frac{\gamma_2\pi}{l}x\right)+C_3x \tag{16}$$

where $\gamma_1 = \sqrt{\beta + \sqrt{\beta^2 - \alpha^2}}$ and $\gamma_2 = \sqrt{\beta - \sqrt{\beta^2 - \alpha^2}}$. Those closed-form expressions in Equation 16 are the infinite sum of Fourier series as derived in Appendix II. C_1, C_2 and C_3 are as follows:

$$C_1 = \frac{c_1}{c_0};\ C_2 = -\frac{c_2}{c_0};\ C_3 = -\frac{B}{2\pi S_3 \alpha^2} \tag{17a-c}$$

$$c_1 = \frac{l^2}{6\pi S_3 \gamma_2^2 \sinh \pi\gamma_1} \left[l^4 S_1 \gamma_2 \left(3\coth \pi\gamma_2 - \pi\gamma_2 \right) - 3 + 6\pi^4 S_3 \gamma_2^4 \left(A\gamma_1^2 - B \right) \right] \tag{17d}$$

$$c_2 = \frac{l^2}{6\pi S_3 \gamma_1^2 \sinh \pi\gamma_2} \left[l^4 S_1 \gamma_1 \left(3\coth \pi\gamma_1 - \pi\gamma_1 \right) - 3 + 6\pi^4 S_3 \gamma_1^4 \left(A\gamma_2^2 - B \right) \right] \tag{17e}$$

$$c_0 = l^4 S_1 \left[\gamma_1\gamma_2 \left(\gamma_1 \coth \pi\gamma_2 - \gamma_2 \coth \pi\gamma_1 \right) - 2\sqrt{\beta^2 - \alpha^2} \right] + 4\pi^4 S_3 \alpha^2 \sqrt{\beta^2 - \alpha^2} \tag{17f}$$

Note that c_2 is obtained by replacing γ_1 with γ_2 in c_1.

2.5. Stage II: transverse normal stress in the adhesive layer

In this section, we only retain the shear stress derived in Section 2.4. Substituting Equations 16 and 5b into Equation 4, we obtain:

$$\sigma_y^{[2]} = \Sigma a_m \cos\frac{m\pi x}{l} - y^{[2]} \left(C_1 \frac{\gamma_1\pi}{l} \cosh\frac{\gamma_1\pi}{l} x + C_2 \frac{\gamma_2\pi}{l} \cosh\frac{\gamma_2\pi}{l} x + C_3 \right) \tag{18}$$

Following the same procedure as described in Stage I, the axial stresses in the plate and the beam will be updated as follows:

$$\sigma_x^{[1,j]} = \frac{y^{[1]} b E_x^{[1,j]}}{I_0^{[1]} E_x^{[1,1]}} \sum_m \left(\frac{l}{m\pi} \right)^2 a_m \left[\left(-1 \right)^m - \cos\frac{m\pi x}{l} \right] + \sigma_{xa}^{[1,j]} \tag{19a}$$

$$\sigma_x^{[3,j]} = \frac{y^{[3]} b E_x^{[3,j]}}{I_0^{[3]} E_x^{[3,1]}} \sum_m \left(\frac{l}{m\pi} \right)^2 a_m \left[\left(-1 \right)^m - \cos\frac{m\pi x}{l} \right] + \sigma_{xa}^{[3,j]} + \sigma_{xb}^{[3,j]} \tag{19b}$$

where

$$\sigma_{xa}^{[1,j]} = \frac{bE_x^{[1,j]}}{E_x^{[1,1]}}\left\{C_1\left\{\frac{l}{\pi\gamma_1}\left[\frac{1}{A_0^{[1]}} - \frac{y^{[1]}\left(h^{[1]} - h_0^{[1]} + \frac{h^{[2]}}{2}\right)}{I_0^{[1]}}\right]\left[\cosh\frac{\gamma_1\pi}{l}x - \cosh\gamma_1\pi\right] + \frac{y^{[1]}h^{[2]}(x-l)}{2I_0^{[1]}}\sinh\gamma_1\pi\right\}\right.$$
$$+ C_2\left\{\frac{l}{\pi\gamma_2}\left[\frac{1}{A_0^{[1]}} - \frac{y^{[1]}\left(h^{[1]} - h_0^{[1]} + \frac{h^{[2]}}{2}\right)}{I_0^{[1]}}\right]\left[\cosh\frac{\gamma_2\pi}{l}x - \cosh\gamma_2\pi\right] + \frac{y^{[1]}h^{[2]}(x-l)}{2I_0^{[1]}}\sinh\gamma_2\pi\right\}$$
$$\left. + C_3\left\{\frac{(l^2 - x^2)}{2A_0^{[1]}} - \frac{y^{[1]}(x-l)\left[h_0^{[1]}(x+l) + h^{[2]}(x-l)\right]}{4I_0^{[1]}}\right\}\right\} \tag{19c}$$

$$\sigma_{xa}^{[3,j]} = \frac{bE_x^{[3,j]}}{E_x^{[3,1]}}\left\{C_1\left\{\frac{l}{\pi\gamma_1}\left[\frac{1}{A_0^{[3]}} - \frac{y^{[1]}\left(h^{[3]} + \frac{h^{[2]}}{2}\right)}{I_0^{[3]}}\right]\left[\cosh\gamma_1\pi - \cosh\frac{\gamma_1\pi}{l}x\right] + \frac{y^{[3]}h^{[2]}(x-l)}{2I_0^{[3]}}\sinh\gamma_1\pi\right\}\right.$$
$$+ C_2\left\{\left\{\frac{l}{\pi\gamma_2}\left[\frac{1}{A_0^{[3]}} - \frac{y^{[1]}\left(h^{[3]} + \frac{h^{[2]}}{2}\right)}{I_0^{[3]}}\right]\left[\cosh\gamma_2\pi - \cosh\frac{\gamma_2\pi}{l}x\right] + \frac{y^{[3]}h^{[2]}(x-l)}{2I_0^{[3]}}\sinh\gamma_2\pi\right\}\right\}$$
$$\left. + C_3\left\{\frac{(l^2 - x^2)}{2A_0^{[3]}} - \frac{y^{[3]}(x-l)\left[h_0^{[3]}(x+l) + h^{[2]}(x-l)\right]}{4I_0^{[3]}}\right\}\right\} \tag{19d}$$

$$\sigma_{xb}^{[3,j]} = \frac{E_x^{[3,j]}}{E_x^{[3,1]}}\left\{\frac{N_0}{A_0^{[3]}} + \frac{y^{[3]}}{I_0^{[3]}}\left[M_l + \frac{q}{2}(l^2 - x^2)\right]\right\} \tag{19e}$$

Rewriting the complementary energy U in Equation 11 using the above updated stresses and minimising it by letting $\partial U/\partial a_m = 0$, we have

$$S_1'\left(\frac{l}{m\pi}\right)^2(1)^m\sum_{j=1,2,\cdots}\left(\frac{l}{j\pi}\right)a_j(1)^j + \left[\frac{S_1'}{2}\left(\frac{l}{m\pi}\right)^4 + S_2'\right]a_m = P_m' \tag{20}$$

where

$$S_1' = \sum_{j=1}^{N_1}\frac{b^2 b^{[1,j]}E_x^{[1,j]}}{(E_x^{[1,1]})^2(I_0^{[1]})^2}\left[(1,i-1)^3 + (1,i)^3\right] + \sum_{j=1}^{N_3}\frac{b^2 b^{[3,j]}E_x^{[3,j]}}{(E_x^{[3,1]})^2(I_0^{[3]})^2}\left[(3,i-1)^3 + (3,i)^3\right] \tag{21a}$$

$$S_2' = \frac{b^{(2)}h^{[2]}}{2E_y^{[2]}} \tag{21b}$$

$$P'_m = \frac{F_1}{m^4} + (-1)^m \left(\frac{F_2}{m^4} + \frac{F_3}{m^2} + \frac{F_4}{m^2 + \gamma_1^2} + \frac{F_5}{m^2 + \gamma_2^2} \right) \tag{21c}$$

The coefficients F_i (i = 1..5) are listed in Appendix III.

By introducing

$$\alpha' = \left(\frac{l}{\pi} \right)^2 \sqrt{\frac{S'_1}{2S'_2}} \tag{22}$$

and following the same procedure as described in Stage I, we obtain:

$$\begin{aligned} \sigma_{y0} = {} & H_1 \sum_m \frac{-1^m}{m^2 + \gamma_1^2} \cos\left(\frac{m\pi}{l} x \right) + H_2 \sum_m \frac{-1^m}{m^2 + \gamma_2^2} \cos\left(\frac{m\pi}{l} x \right) \\ & + H_3 \sum_m \frac{(-1)^m}{m^2 + (\eta + I\eta)^2} \cos\left(\frac{m\pi}{l} x \right) + H_4 \sum_m \frac{(-1)^m}{m^2 + (\eta - I\eta)^2} \cos\left(\frac{m\pi}{l} x \right) \\ & + H_5 \sum_m \frac{1}{m^2 + (\eta + I\eta)^2} \cos\left(\frac{m\pi}{l} x \right) + H_6 \sum_m \frac{1}{m^2 + (\eta - I\eta)^2} \cos\left(\frac{m\pi}{l} x \right) \end{aligned} \tag{23}$$

where $\eta = \sqrt{\alpha'/2}$ is a dimensionless parameter and I is the square root of -1. Note that H_i (i = 1..6) are normally complex numbers. Closed-form expressions of the infinite Fourier series in Equation 23 are derived in Appendix II.

By simplifying Equation 23, the imaginary components will automatically vanish, leaving the real components representing the transverse normal stress in the MA section as

$$\begin{aligned} \sigma_{y0} = \frac{1}{S'_2} \Bigg\{ & -G_{1I} \frac{F_1}{\alpha'} + G_{2R} \left(F_3 + \frac{\alpha'^2}{\delta_{11}\delta_{12}} F_4 + \frac{\alpha'^2}{\delta_{21}\delta_{22}} F_5 - \frac{l^2}{\pi^2} S'_1 R' \right) \\ & + G_{2I} \left[-\frac{F_3 F_2}{\alpha'} + \frac{\alpha' \gamma_1^2}{\delta_{11}\delta_{12}} F_4 + \frac{\alpha' \gamma_2^2}{\delta_{21}\delta_{22}} F_5 \right] + G'_1 \frac{\gamma_1^4}{\delta_{11}\delta_{12}} F_4 + G'_2 \frac{\gamma_2^4}{\delta_{21}\delta_{22}} F_5 \Bigg\} \end{aligned} \tag{24}$$

where

$$G_{1I}=\frac{\pi\left[\sin\eta\left(\frac{\pi x}{l}-\pi\right)\cosh\eta\left(\frac{\pi x}{l}+\pi\right)-\sin\eta\left(\frac{\pi x}{l}+\pi\right)\cosh\eta\left(\frac{\pi x}{l}-\pi\right)+\cos\eta\left(\frac{\pi x}{l}-\pi\right)\sinh\eta\left(\frac{\pi x}{l}+\pi\right)-\cos\eta\left(\frac{\pi x}{l}+\pi\right)\sinh\eta\left(\frac{\pi x}{l}-\pi\right)\right]}{4\eta\left(\cosh 2\pi\eta-\cos 2\pi\eta\right)}$$

$$G_{2R}=\frac{\pi\left[\sin\eta\left(\frac{\pi x}{l}-2\pi\right)\cosh\eta\pi-\sin\eta\pi\cosh\eta\left(\frac{\pi x}{l}-2\pi\right)+\cos\eta\pi\sinh\eta\left(\frac{\pi x}{l}-2\pi\right)-\cos\eta\left(\frac{\pi x}{l}-2\pi\right)\sinh\eta\pi\right]}{4\eta\left(\cosh 2\pi\eta-\cos 2\pi\eta\right)}+\frac{1}{4\eta^2}$$

$$G_{2I}=\frac{\pi\left[\sin\eta\left(\frac{\pi x}{l}-\pi\right)\cosh\eta\left(\frac{\pi x}{l}+\pi\right)-\sin\eta\left(\frac{\pi x}{l}+\pi\right)\cosh\eta\left(\frac{\pi x}{l}-\pi\right)+\cos\eta\left(\frac{\pi x}{l}+\pi\right)\sinh\eta\left(\frac{\pi x}{l}-\pi\right)-\cos\eta\left(\frac{\pi x}{l}-\pi\right)\sinh\eta\left(\frac{\pi x}{l}+\pi\right)\right]}{4\eta\left(\cosh 2\pi\eta-\cos 2\pi\eta\right)}+\frac{1}{4\eta^2}$$

$$G_1'=\frac{\pi\cosh\gamma_1\dfrac{\pi x}{l}}{2\gamma_1\sin\gamma_1\pi}-\frac{1}{2\gamma_1^2}$$

$$G_2'=\frac{\pi\cosh\gamma_2\dfrac{\pi x}{l}}{2\gamma_2\sin\gamma_2\pi}-\frac{1}{2\gamma_2^2} \qquad \text{(25a-e)}$$

$$\delta_{11}=\gamma_1^2-2\eta\gamma_1+\alpha' \qquad \text{(25f)}$$

$$\delta_{12}=\gamma_1^2+2\eta\gamma_1+\alpha' \qquad \text{(25g)}$$

$$\delta_{21}=\gamma_2^2-2\eta\gamma_2+\alpha' \qquad \text{(25h)}$$

$$\delta_{22}=\gamma_2^2+2\eta\gamma_2+\alpha' \qquad \text{(25i)}$$

And $R^{'}$ is presented in Appendix III.

Using Equation 18, the interfacial normal stress can be obtained by substituting $y^{[2]}$ with $h^{[2]}/2$ and $-h^{[2]}/2$, respectively.

$$\sigma_y^{(1)}=\sigma_{y0}-\frac{h^{[2]}}{2}\left(C_1\frac{\gamma_1\pi}{l}\cosh\frac{\gamma_1\pi}{l}x+C_2\frac{\gamma_2\pi}{l}\cosh\frac{\gamma_2\pi}{l}x+C_3\right) \qquad \text{(26a)}$$

$$\sigma_y^{(2)}=\sigma_{y0}+\frac{h^{[2]}}{2}\left(C_1\frac{\gamma_1\pi}{l}\cosh\frac{\gamma_1\pi}{l}x+C_2\frac{\gamma_2\pi}{l}\cosh\frac{\gamma_2\pi}{l}x+C_3\right) \qquad \text{(26b)}$$

3. Numerical examples

The first example is an RC beam bonded with a steel plate subjected to a UDL q = 15N/mm (see Figure 3). The beam, having 2.4m span and a rectangular section of 150mm thickness and 100mm width, was initially analyzed by Roberts and Haji-Kazemi [9]. The bonded plate is 1800mm long and 4mm thick and has the same width as the

beam. The plate is fully bonded to the RC beam with a 4mm thick adhesive layer. The Young's moduli are 20 GPa for concrete and 200 GPa for the bonded steel plate. The adhesive is treated as an isotropic material with Young's modulus $E^{[2]}$ =2GP and Poisson's ratio $\nu^{[2]}$ = 0.3. This example has been studied in various studies [8, 20-25]. It is revisited here to verify the present solution. Like other solutions, the effect of steel reinforcing bars is ignored and hence only one layer is considered for both the RC beam and the steel plate. For comparison purpose, this example is also analyzed using FE method by the general purpose FEA package ABAQUS [26]. Figure 4 shows the mesh pattern of the analysis where converged results were obtained. Both results are presented in Figure 5.

The comparison of the transverse normal stress indicates that both methods predict a tensile stress at the AB interface and a compressive one at the PA interface. The peak values at both interfaces predicted by the present solution are lower than those from the FEA. Because of the stress singularity at the plate end, the peak value, in theory, should approach infinity. Unless a singular solution is introduced, no elastic approaches including FEA can yield an infinite peak value. However, the singularity only affect very small zone, i.e. the close vicinity of the plate end. It can be seen from Figure 5 that both results show satisfactory coincidence except for the zone very close to the plate end. A single shear stress distribution is predicted by the present solution, and as Figure (5b) shows, its peak value is slightly lower than those from the FEA method at both interfaces and the MA section.

The second verification example is taken from Shen et al. [20]. An RC beam is bonded with a CFRP plate and subjected to UDL with q = 15N/mm. Geometrical and material properties of the strengthened beam are: L = 1500mm, l = 1200mm, $h^{[1]}$= $h^{[2]}$= 2mm, $h^{[3]}$= 300mm, b = $b^{[3]}$ = 200mm, $E_x^{[1]}$= 140GPa, $E_x^{[3]}$ = 30GPa, $E_x^{[2]}$ = $E_y^{[2]}$= 3GPa and $\nu_{xy}^{[2]}$ = 0.35. Results from the present solution and Shen et al.'s are both presented in Figure 6. As Figure 6(a) shows, Shen et al.'s solution predicted a monotonically increased normal stress in both AB and PA interfaces. However, the stress at the PA interface should reach

its peak value at a location near, but not at the free end as revealed in the FEA analysis[24, 25]. The present solution has shown the same trend as FEA does. In Figure (6b), both solutions predict almost identical shear stresses. Shen et al's results suggested that there was little difference in the interfacial shear stresses between AB and PA interfaces[20]. This observation forms the basis of the assumption adopted in deriving the present solution that the shear stress is constant over thickness.

The third example is a cast iron (CI) beam strengthened with CFRP and subject to a uniform temperature rise of 30 ^{o}C. The beam was originally analyzed by Stratford and Cadei [13]. The cross section and its dimension are given in Figure 7.

The whole beam spans 6m and the bonded part is 4m long. The thickness of the adhesive is 2mm and that of the CFRP plate is 11mm. The adhesive and the CFRP share the same width as that of the bottom flange of the CI beam. The material properties are: $E_x^{[1]}$ = 360GPa, $E_x^{[3]}$ = 138GPa, $E_x^{[2]} = E_y^{[2]}$ = 4.5GPa, $\nu_{xy}^{[2]}$ = 0.32, and the coefficient of expansion is $\alpha^{[1]}$ = 1 x 10^{-6} /^{o}C, $\alpha^{[3]}$ = 11 x 10^{-6} /^{o}C. Because of the different thermal expansion between the beam and the plate, significant thermal stresses can arise in the plated beam due to a temperature raise (or drop). For a simply supported plated beam subjected to a uniform temperature gradient over the thickness, the thermal effect can be treated as a combination of a pair of equivalent axial force N_0 and bending moment M_0 applied at both ends of the beam:

$$N_0 = \sum_{j=i}^{N_3} E_{[i,j]} b_{[i,j]} \left\{ \frac{\left[y_{(3,j-1)}^2 - y_{(3,j)}^2 \right]}{2} \frac{\alpha^{[3]} (\Delta T_b - \Delta T_t)}{h_{[i]}} + \alpha^{[3]} \left[\frac{h_0 (\Delta T_t - \Delta T_b)}{h_{[i]}} + \Delta T_b \right] h_{[i,j]} \right\} \tag{20a}$$

$$M_0 = -\sum_{j=i}^{N_3} E_{[i,j]} b_{[i,j]} \left\{ \frac{\left[y_{(3,j-1)}^3 - y_{(3,j)}^3 \right]}{3} \frac{\alpha^{[3]} (\Delta T_b - \Delta T_t)}{h_{[i]}} + \frac{\left[y_{(3,j-1)}^2 - y_{(3,j)}^2 \right]}{2} \alpha^{[3]} \left[\frac{h_0 (\Delta T_t - \Delta T_b)}{h_{[i]}} + \Delta T_b \right] \right\} \tag{20b}$$

in which ΔT_t = the temperature rise at the top of the strengthened beam; ΔT_b = the temperature rise at the bottom of the strengthened beam. These equivalent mechanical loads are formulated by assuming a same deformation caused by the thermal effect and the equivalent mechanical loads.

In this example, the beam is divided into three sub-layers, the bottom flange, the web and the top flange. They have different width and thickness but share the same material property. Figure 8 shows the comparisons of the results obtained from the present method and Stratford and Cadei's [132] approximate method. It is apparent that the agreement is very positive. In their method, only uniform normal and shear stresses were obtained. In the present solution, there is a significant difference in the normal stress along the PA interface, the AB interface and the MA section, in particular, near the plate end. It can be seen from Figure 8a that the approximate solution of the transverse normal stress from Stratford and Cadei's method is close to the stress in the MA section obtained in the present approach. Only one shear stress is predicated by both present and approximate solutions. As expected, the approximate solution of shear stress increases monotonically whereas the present solution satisfies the zero shear stress condition at the plate end.

The last example is to investigate the effect of including the steel reinforcement in a RC beam bonded with CFRP. The beam is subjected to a UDL of q = 30N/mm and has the cross section as shown in Figure 9. Steel reinforcements of 12mm in diameter are included and the cover is 25mm. The span of the simply-supported beam is 3m and the bonded part is 2.4m long. The thickness of the adhesive layer is 2mm and that of the CFRP is 3mm. Both the adhesive layer and the CFRP share the same width as the RC beam. The Young's moduli for the concrete is 30 GPa, for the steel is 205GPa, for the adhesive is 3GPa and for the CFRP is 200GPa. The Poisson's ratio for adhesive $\nu_{xy}^{[2]}$ = 0.35. A fictitious layer including the reinforcement is defined with the thickness as twice as the diameter of the reinforcement, i.e. 24mm. Hence the concrete beam is divided into three sub-layers. It is apparent that each layer has the same width but the one with rebars has different material property. The Young's modulus in the sub-layer containing the steel reinforcement is calculated as the weighted average value from the plain concrete and the steel. The weight is taken as the volume ratio. Three cases are analyzed, i.e. including 0, 3 and 6 bars, which results in three different reinforcement ratios, i.e. 0, 0.8% and 1.6%, respectively.

Figures 10(a) and (b) present, respectively, the transverse normal and shear stresses in these three cases. It can be seen that with higher reinforcement ratio, the peak values for all stresses are reduced. It is interesting to find that the reduction of peak values in percentage for 0.8% reinforcement ratio is 10% and for 1.6% reinforcement ratio is 17% in all studied stresses.

Figure 10(c) presents a 3-D graph showing the distribution of the transverse normal stress within the adhesive layer when a 0.8% reinforcement ratio is considered in the calculation. It reveals that the stress varies drastically in the close vicinity of the end of the adhesive layer.

4. Conclusions

In this paper, an improved closed-form interfacial stress formulation is developed for plated beams. This formulation has the following favourable features in comparison with exiting analytical solutions:

(a) It provides results for both interfacial shear and normal stresses with improved accuracy compared with most approximate solutions;

(b) Due to the nature of closed form, the present solution can be readily used to obtain numerical results by only utilizing simple spreadsheet packages, and the numeric overflow problems does not exit;

(c) It is the first closed-form solution that satisfies the traction-free boundary condition and predicts the non-monotonic normal stress at the PA interface;

(d) It can be further exploited to develop a simplified version, so that a design-oriented strength model can be established based on more compact stress results;

(e) It is versatile in nature and can be used to analyze any beams and bonded plates by introducing sub-layers;

(f) Thermal effects can be included by using equivalent mechanical loads.

Three widely quoted examples have been re-analyzed by using the present method and the agreement is satisfactory. Numerical results have revealed that the interfacial stresses

obtained without considering the steel reinforcement are over-estimated, and increasing the reinforcement ratio will reduce the peak value of interfacial stresses.

Acknowledgement

The authors wish to thank Dr. Gordon Little for his constructive comments during preparing this paper.

Appendix I. Derivation of the coefficient ξ as defined in Equation (6)

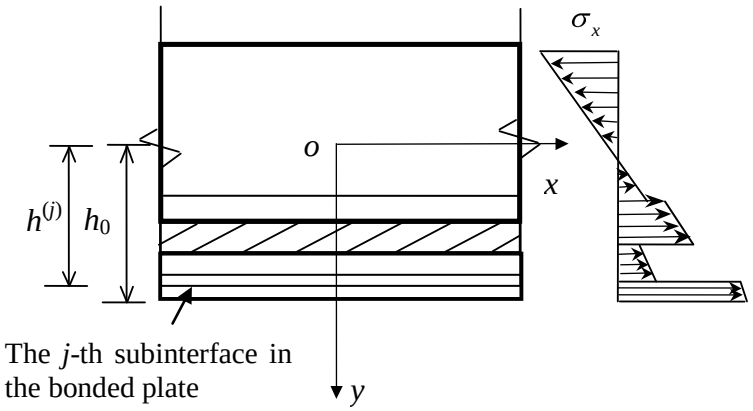

Fig. A1.1 The longitudinal stress over the composite cross section of the bonded beam using CLBT

The longitudinal stress over the composite cross section, σ_x can be obtained by the classical laminate beam theory (CLBT) [27] (see Figure A1.1) as

$$\sigma_x = \frac{M_z}{I_0}\frac{E_x^{[i,j]}}{E_x^{[1,1]}}y \tag{A1.1}$$

where M_z is the internal bending moment on the cross section, y is the vertical coordinate from the neutral axis; I_0 is the second moment of area of the entire cross-section transformed to the material of the first sub-layer of the plate, i.e.

$$I_0 = \frac{1}{12}\sum_{i=1,3}\left(\sum_{j=1}^{N_i} b^{[i,j]}\frac{E_x^{[i,j]}}{E_x^{[1,1]}}\left(h^{[i,j]}\right)^3\right) + \sum_{j=1}^{N_1}\left[b^{[1,j]}\frac{E_x^{[1,j]}}{E_x^{[1,1]}}h^{[1,j]}\left(\sum_{k=1}^{j}h^{[1,k]} - \frac{h^{[1,j]}}{2} - h_0\right)^2\right] + \sum_{j=1}^{N_3}\left[b^{[3,j]}\frac{E_x^{[3,j]}}{E_x^{[1,1]}}h^{[3,j]}\left(h^{[1]} + h^{[2]} + \sum_{k=1}^{j}h^{[3,k]} - \frac{h^{[3,j]}}{2} - h_0\right)^2\right]$$
$$+\frac{1}{12}b\frac{E_x^{[2]}}{E_x^{[1,1]}}\left(h^{[2j]}\right)^3 + b\frac{E_x^{[2]}}{E_x^{[1,1]}}h^{[2]}\left(h^{[1]} + \frac{h^{[2]}}{2} - h_0\right)^2 \tag{A1.2}$$

In equation (A1.2) h_0 is the distance from the neutral axis to the lower surface of the transferred cross-section, i.e.

$$h_0 = \frac{\sum_{j=1}^{N_1} b^{[1,j]} \frac{E_x^{[1,j]}}{E_x^{[1,1]}} h^{[1,j]} \left(\sum_{k=1}^{j} h^{[1,k]} - \frac{h^{[1,j]}}{2} \right) + \sum_{j=1}^{N_3} b^{[3,j]} \frac{E_x^{[3,j]}}{E_x^{[1,1]}} h^{[3,j]} \left(h^{[1]} + h^{[2]} + \sum_{k=1}^{j} h^{[3,k]} - \frac{h^{[3,j]}}{2} \right) + b \frac{E_x^{[2]}}{E_x^{[1,1]}} h^{[2]} \left(h^{[1]} + \frac{h^{[2]}}{2} \right)}{A_0} \tag{A1.3}$$

where A_0 is the transformed cross sectional area

$$A_0 = \sum_{j=1}^{N_1} b^{[1,j]} \frac{E_x^{[1,j]}}{E_x^{[1,1]}} h^{[1,j]} + \sum_{j=1}^{N_3} b^{[3,j]} \frac{E_x^{[3,j]}}{E_x^{[1,1]}} h^{[3,j]} + b \frac{E_x^{[2]}}{E_x^{[1,1]}} h^{[2]} \tag{A1.4}$$

The stress resultants due to σ_x in the bonded plate with respect to its own neutral axis are

$$N^{[1]} = \sum_{j=1}^{N_1} b^{[1,j]} \frac{E_x^{[1,j]}}{E_x^{[1,1]}} \frac{M_z}{I_0} \int_{h^{(j)}}^{h^{(j-1)}} y dy = \frac{M_z}{I_0 E_x^{[1,1]}} \sum_{j=1}^{N_1} b^{[1,j]} E_x^{[1,j]} \frac{\left(h^{(j-1)}\right)^2 - \left(h^{(j)}\right)^2}{2} \tag{A1.5a}$$

$$M^{[1]} = \sum_{j=1}^{N_1} b^{[1,j]} \frac{E_x^{[1,j]}}{E_x^{[1,1]}} \frac{M_z}{I_0} \int_{h^{(i)}}^{h^{(i-1)}} y \left(y - h_0 + h_0^{[1]}\right) dy = \frac{M_z}{I_0 E_x^{[1,1]}} \sum_{j=1}^{N_1} b^{[1,j]} E_x^{[1,j]} \left\{ \frac{\left(h^{(j-1)}\right)^3 - \left(h^{(j)}\right)^3}{3} - \left(h_0 - h_0^{[1]}\right) \frac{\left(h^{(j-1)}\right)^2 - \left(h^{(j)}\right)^2}{2} \right\} \tag{A1.5b}$$

where $h^{(j)}$ is the y-coordinate of the j-th sub-interface of the plate in the coordinate system defined for the transformed cross section. Figure A1.1 shows such a coordinate system, where the origin is located at the centroid of the transferred cross section. The plate and the beam may contain sub-layers.

These two stress resultants can also be obtained by considering the equilibrium and boundary conditions of the plate in Equations 1 and 2 and can be represented by the Fourier series in Equation 5, i.e.

$$N^{[1]} = \sum_m \frac{lbb_m}{m\pi} \left[\left(-1\right)^m - \cos\frac{m\pi x}{l} \right] \tag{A1.6a}$$

$$M^{[1]} = \sum_m \frac{lbb_m}{2m\pi} \left[\left(-1\right)^m - \cos\frac{m\pi x}{l} \right] \left(\xi - h^{[1]} - h^{[2]}\right) \tag{A1.6b}$$

It is noted that in Equation A1.6b, a_m is replaced by $\xi \left(m\pi / l\right) b_m$ based on the definition of ξ in Equation 6. Combining Equations A1.5 and A1.6 and eliminating $N^{[1]}$ and $M^{[1]}$, one obtains

$$\sum_{j=1}^{N_1} b^{[1,j]} E_x^{[1,j]} \left\{ \frac{\left[\left(\xi^{(j-1)}\right)^3 - \left(\xi^{(j)}\right)^3 \right]}{3} - \left(\xi_0 - h_0^{[1]}\right) \frac{\left[\left(\xi^{(j-1)}\right)^2 - \left(\xi^{(j)}\right)^2 \right]}{2} \right\} \sum_m \frac{b_m}{m} \left[\left(-1\right)^m - \cos\frac{m\pi x}{l} \right] =$$

$$\sum_{j=1}^{N_1} b^{[1,j]} E_x^{[1,j]} \frac{\left[\left(\xi^{(j1)}\right)^2 - \left(\xi^{(j)}\right)^2 \right]}{2} \left(\xi - h^{[1]} - h^{[2]}\right) \sum_m \frac{b_m}{m} \left[\left(-1\right)^m - \cos\frac{m\pi x}{l} \right] \qquad \text{(A1.10)}$$

By equating the series term-by-term, we have

$$\xi = \frac{1}{2} \left\{ \frac{\sum_{j=1}^{N_1} b^{[1,j]} E_x^{[1,j]} \left\{ \frac{\left[\left(\xi^{(j-1)}\right)^3 - \left(\xi^{(j)}\right)^3 \right]}{3} - \left(\xi_0 - h_0^{[1]}\right) \frac{\left[\left(\xi^{(j-1)}\right)^2 - \left(\xi^{(j)}\right)^2 \right]}{2} \right\} \sum_m \frac{b_m}{m} \left[\left(-1\right)^m - \cos\frac{m\pi x}{l} \right]}{\sum_{j=1}^{N_1} b^{[1,j]} E_x^{[1,j]} \frac{\left[\left(\xi^{(j1)}\right)^2 - \left(\xi^{(j)}\right)^2 \right]}{2}} + h^{[1]} + h^{[2]} \right\} \qquad \text{(A1.11)}$$

Appendix II. The infinite sum of Fourier series

The infinite sums of Fourier series used in this study are listed as follows:

$$\sum_m \frac{1}{m^2 + a^2} \cos(mx) = \frac{\pi}{2a} \frac{\cosh a\left(\pi - x\right)}{\sinh a\pi} - \frac{1}{2a^2}, \; 0 \le x \le 2\pi \qquad \text{(A2.1a)}$$

$$\sum_m \frac{\left(-1\right)^m}{m^2 + a^2} \cos(mx) = \frac{\pi}{2a} \frac{\cosh ax}{\sinh a\pi} - \frac{1}{2a^2}, 0 \le x \le 2\pi \qquad \text{(A2.1b)}$$

$$\sum_m \frac{m}{m^2 + a^2} \sin(mx) = \begin{cases} -\frac{\pi}{2} \frac{\sinh a \;\; \pi + x}{\sinh a\pi}, & -\pi \le x < 0 \\ 0 & x = 0 \\ \frac{\pi}{2} \frac{\sinh a \;\; \pi - x}{\sinh a\pi}, & 0 < x \le \pi \end{cases} \qquad \text{(A2.1c)}$$

$$\sum_m \frac{-1^{\;m} m}{m^2 + a^2} \sin(mx) = \begin{cases} -\frac{\pi}{2} \frac{\sinh ax}{\sinh a\pi}, & -\pi < x < \pi \\ 0, & \pm\pi \end{cases} \qquad \text{(A2.1d)}$$

where a is an arbitrary real constant, and m is a non-negative integer, i.e., $m = 0, 1, 2, \ldots$ These equations are only valid for above-specified domains. For x values out of valid domains, we can conduct simple transformation in order to utilize the above equations. For example, if x is given in the range of $-2\pi \le x \le 0$, in order to use Equation A2.1a, we introduce another variable X and let $X = x + 2\pi$. Thus

$$\sum_m \frac{1}{m^2 + a^2} \cos(mx) = \sum_m \frac{1}{m^2 + a^2} \cos(mX)$$

$$\frac{\pi}{2a}\frac{\cosh a(\pi - X)}{\sinh a\pi} - \frac{1}{2a^2} = \frac{\pi}{2a}\frac{\cosh a(\pi + x)}{\sinh a\pi} - \frac{1}{2a^2}, -2\pi \le x \le 0 \quad \text{(A2.3e)}$$

The infinite sum of series in Equations (15d) and (15e) can be transformed into their partial fraction forms, i.e.

$$\sum_m \frac{1}{m^4 + 2\beta m^2 + \alpha^2} = \sum_m \frac{1}{(m^2 + \gamma_1^2)(m^2 + \gamma_2^2)} = \frac{1}{\gamma_1^2 - \gamma_2^2}\left[\sum_m \frac{1}{(m^2 + \gamma_2^2)} - \sum_m \frac{1}{(m^2 + \gamma_1^2)}\right] \quad \text{(A2.2a)}$$

$$\sum_m \frac{1}{m^2\ (m^4 + 2\beta m^2 + \alpha^2)} = \sum_m \frac{1}{m^2\ (m^2 + \gamma_1^2\ \ m^2 + \gamma_2^2)}$$

$$= \frac{1}{\gamma_1^2 - \gamma_2^2}\left[\frac{1}{\gamma_1^2}\sum_m \frac{1}{m^2 + \gamma_1^2} - \frac{1}{\gamma_2^2}\sum_m \frac{1}{m^2 + \gamma_2^2}\right] + \frac{1}{\gamma_1^2\gamma_2^2}\sum_m \frac{1}{m^2} \quad \text{(A2.2b)}$$

where $\gamma_1 = \sqrt{\beta + \sqrt{\beta^2 - \alpha^2}}$ and $\gamma_2 = \sqrt{\beta - \sqrt{\beta^2 - \alpha^2}}$.

Equations A2.2 can be obtained by substituting appropriate values to *x* and *a* in Equations A2.1. For instance, by substituting *x* = 0 and $a = \gamma_1$ into Equation A2.1a, we have

$$\sum_m \frac{1}{m^2 + \gamma_1^2} = \frac{\pi}{2\gamma_1}\frac{\cosh \gamma_1\pi}{\sinh \gamma_1\pi} - \frac{1}{2\gamma_1^2} \quad \text{(A2.3 a)}$$

The limit of Equation A2.3 a when $\gamma_1 \to 0$ yields

$$\sum_m \frac{1}{m^2} = \frac{\pi^2}{6} \quad \text{(A2.3 b)}$$

Equations A2.1 is also valid when *a* is a complex number, e.g. a substitution of *a* by *c* + *Id* in Equations A2.1 (a) and (b), yields

$$\sum_m \frac{1}{m^2 + (c + Id)^2}\cos mx = G_{1R} + IG_{1I} \quad \text{(A2.5 a)}$$

$$\sum_m \frac{(-1)^m}{m^2 + (c + Id)^2}\cos mx = G_{2R} + IG_{2I} \quad \text{(A2.5 b)}$$

where

$$G_{1R}=\frac{1}{2(c^2+d^2)}\left\{\pi\left[\frac{c(\sinh cx\cos d(x-2\pi)-\sinh c(x-2\pi)\cos dx)+d(\cosh cx\sin d(x-2\pi)-\cosh c(x-2\pi)\sin dx)}{\cos 2\pi c-\cos 2\pi d}\right]-\frac{c^2-d^2}{c^2+d^2}\right\}$$

$$G_{1I}=\frac{1}{2(c^2+d^2)}\left\{-\pi\left[\frac{c(\cosh cx\sin d(x-2\pi)+\cosh c(x-2\pi)\sin dx)+d(\sinh cx\cos d(x-2\pi)+\sinh c(x-2\pi)\cos dx)}{\cos 2\pi c-\cos 2\pi d}\right]+\frac{cd}{c^2+d^2}\right\}$$

$$G_{2R}=\frac{1}{2(c^2+d^2)}\left\{\pi\left[\frac{c(\sinh c(x+\pi)\cos d(x-\pi)-\sinh c(x-\pi)\cos d(x+\pi))+d(\cosh c(x+\pi)\sin d(x-\pi)-\cosh c(x-\pi)\sin d(x+\pi))}{\cos 2\pi c-\cos 2\pi d}\right]-\frac{c^2-d^2}{c^2+d^2}\right\}$$

$$G_{2I}=\frac{1}{2(c^2+d^2)}\left\{-\pi\left[\frac{c(\cosh c(x+\pi)\sin d(x-\pi)+\cosh c(x-\pi)\sin d(x+\pi))+d(\sinh c(x+\pi)\cos d(x-\pi)+\sinh c(x-\pi)\cos d(x+\pi))}{\cos 2\pi c-\cos 2\pi d}\right]+\frac{cd}{c^2+d^2}\right\}$$

(A2.6a-d)

Appendix III. Coefficients in Equations (13d), (21c) and (24)

In Equations (13d) and (21c)

$$A=\frac{blN_0}{\pi(E_x^{[3,1]})A_0^{[3]}}\left[\frac{\sum_{j=1}^{N_3}b^{[3,j]}E_x^{[3,j]}\varepsilon_5^{[j]}}{A_0^{[3]}}+\frac{\kappa_0\sum_{j=1}^{N_3}b^{[3,j]}E_x^{[3,j]}\varepsilon_4^{[j]}}{I_0^{[3]}}\right]+\frac{bl\kappa_0}{\pi(E_x^{[3,1]})I_0^{[3]}}\left[M_0+\frac{q(c^2-l^2)}{2}\right]\left[\frac{2\sum_{j=1}^{N_3}b^{[3,j]}E_x^{[3,j]}\varepsilon_4^{[j]}}{A_0^{[3]}}+\frac{\sum_{j=1}^{N_3}b^{[3,j]}E_x^{[3,j]}\varepsilon_2^{[j]}}{I_0^{[3]}}\right]$$

$$+\frac{bl^3q}{3\pi(E_x^{[3,1]})I_0^{[3]}}\left(\frac{\kappa_0\sum_{j=1}^{N_3}b^{[3,j]}E_x^{[3,j]}\varepsilon_2^{[j]}}{I_0^{[3]}}+\frac{2\sum_{j=1}^{N_3}b^{[3,j]}E_x^{[3,j]}\varepsilon_4^{[j]}}{A_0^{[3]}}\right)$$

$$B=\frac{bl^3q}{\pi^3(E_x^{[3,1]})I_0^{[3]}}\left(\frac{\kappa_0\sum_{j=1}^{N_3}b^{[3,j]}E_x^{[3,j]}\varepsilon_2^{[j]}}{I_0^{[3]}}+\frac{2\sum_{j=1}^{N_3}b^{[3,j]}E_x^{[3,j]}\varepsilon_4^{[j]}}{A_0^{[3]}}\right) \qquad \text{(A3.1-2)}$$

$$F_1=\frac{b^2l^3h^{[2]}}{\pi^4}(C_1\sinh\gamma_1\pi+C_2\sinh\gamma_2\pi+C_3l)\left[\frac{\sum_{j=1}^{N_3}b^{[3,j]}E_x^{[3,j]}\varepsilon_2^{[j]}}{(E_x^{[3,1]})(I_0^{[3]})}-\frac{\sum_{j=1}^{N_1}b^{[1,j]}E_x^{[1,j]}\varepsilon_1^{[j]}}{(E_x^{[1,1]})(I_0^{[1]})}\right]$$

$$F_2=\frac{b^2l^3h^{[2]}}{\pi^4}(C_1\sinh\gamma_1\pi+C_2\sinh\gamma_2\pi)\left[\frac{\sum_{j=1}^{N_1}b^{[1,j]}E_x^{[1,j]}\varepsilon_1^{[j]}}{(E_x^{[1,1]})(I_0^{[1]})}-\frac{\sum_{j=1}^{N_3}b^{[3,j]}E_x^{[3,j]}\varepsilon_2^{[j]}}{(E_x^{[3,1]})(I_0^{[3]})}\right]$$

$$+\frac{b^2l^4C_3}{\pi^4}\left[\sum_{j=1}^{N_1}b^{[1,j]}E_x^{[1,j]}\varepsilon_1^{[j]}\frac{(I_0^{[1]}-h^{[1]})}{(E_x^{[1,1]})(I_0^{[1]})}+\frac{\sum_{j=1}^{N_1}b^{[1,j]}E_x^{[1,j]}\varepsilon_3^{[j]}}{(E_x^{[1,1]})A_0^{[1]}I_0^{[1]}}+\sum_{j=1}^{N_3}b^{[3,j]}E_x^{[3,j]}\varepsilon_2^{[j]}\frac{(I_0^{[3]})}{(E_x^{[3,1]})(I_0^{[3]})}+\frac{\sum_{j=1}^{N_3}b^{[3,j]}E_x^{[3,j]}\varepsilon_4^{[j]}}{(E_x^{[3,1]})A_0^{[3]}I_0^{[3]}}\right]$$

$$+\frac{2bl^4q}{\pi^4(E_x^{[3,1]})(I_0^{[3]})}\sum_{j=1}^{N_3}b^{[3,j]}E_x^{[3,j]}\varepsilon_2^{[j]}$$

$$F_3 = \frac{b^2 l^3 h^{[2]}}{2\pi^2}\left(C_1 \sinh\gamma_1\pi + C_2 \sinh\gamma_2\pi\right)\left[\frac{\sum_{j=1}^{N_1} b^{[1,j]} E_x^{[1,j]} \varepsilon_1^{[j]}}{E_x^{[1,1]} I_0^{[1]}} - \frac{\sum_{j=1}^{N_3} b^{[3,j]} E_x^{[3,j]} \varepsilon_2^{[j]}}{E_x^{[3,1]} I_0^{[3]}}\right]$$

$$+\frac{b^2 l^3}{\pi^3}\left(C_1 \frac{\cosh\gamma_1\pi}{\gamma_1} + C_2 \frac{\cosh\gamma_2\pi}{\gamma_2}\right)\left[\frac{\kappa_1 \sum_{j=1}^{N_1} b^{[1,j]} E_x^{[1,j]} \varepsilon_1^{[j]}}{E_x^{[1,1]} I_0^{[1]}} + \frac{\kappa_2 \sum_{j=1}^{N_3} b^{[3,j]} E_x^{[3,j]} \varepsilon_2^{[j]}}{E_x^{[3,1]} I_0^{[3]}} + \frac{\sum_{j=1}^{N_1} b^{[1,j]} E_x^{[1,j]} \varepsilon_3^{[j]}}{E_x^{[1,1]} A_0^{[1]} I_0^{[1]}} + \frac{\sum_{j=1}^{N_3} b^{[3,j]} E_x^{[3,j]} \varepsilon_4^{[j]}}{E_x^{[3,1]} A_0^{[3]} I_0^{[3]}}\right]$$

$$+\frac{b^2 l^4 C_3}{\pi^2}\left[\frac{\kappa_3 \sum_{j=1}^{N_1} b^{[1,j]} E_x^{[1,j]} \varepsilon_1^{[j]}}{E_x^{[1,1]} I_0^{[1]}} + \frac{2\sum_{j=1}^{N_1} b^{[1,j]} E_x^{[1,j]} \varepsilon_3^{[j]}}{3E_x^{[1,1]} A_0^{[1]} I_0^{[1]}} + \frac{\kappa_4 \sum_{j=1}^{N_3} b^{[3,j]} E_x^{[3,j]} \varepsilon_2^{[j]}}{E_x^{[3,1]} I_0^{[3]}} + \frac{2\sum_{j=1}^{N_3} b^{[3,j]} E_x^{[3,j]} \varepsilon_4^{[j]}}{3E_x^{[3,1]} A_0^{[3]} I_0^{[3]}}\right]$$

$$+\frac{2bl^2 N_0}{\pi^2 E_x^{[3,1]} A_0^{[3]} I_0^{[3]}} \sum_{j=1}^{N_3} b^{[3,j]} E_x^{[3,j]} \varepsilon_4^{[j]} + \frac{2bl^2}{\pi^2 E_x^{[3,1]} I_0^{[3]}}\left[M_0 + \frac{q\left(\xi^2 - l^2\right)}{2}\right]\sum_{j=1}^{N_3} b^{[3,j]} E_x^{[3,j]} \varepsilon_2^{[j]} + \frac{2bl^4 q}{3\pi^2 E_x^{[3,1]} I_0^{[3]}} \sum_{j=1}^{N_3} b^{[3,j]} E_x^{[3,j]} \varepsilon_2^{[j]}$$

$$F_4 = \frac{2b^2 l^3 C_1 \sinh\gamma_1\pi}{\pi^4 \gamma_1^2}\left[-\frac{\kappa_1 \sum_{j=1}^{N_1} b^{[1,j]} E_x^{[1,j]} \varepsilon_1^{[j]}}{E_x^{[1,1]} I_0^{[1]}} - \frac{\sum_{j=1}^{N_1} b^{[1,j]} E_x^{[1,j]} \varepsilon_3^{[j]}}{E_x^{[1,1]} A_0^{[1]} I_0^{[1]}} - \frac{\kappa_2 \sum_{j=1}^{N_3} b^{[3,j]} E_x^{[3,j]} \varepsilon_2^{[j]}}{E_x^{[3,1]} I_0^{[3]}} - \frac{\sum_{j=1}^{N_3} b^{[3,j]} E_x^{[3,j]} \varepsilon_4^{[j]}}{E_x^{[3,1]} A_0^{[3]} I_0^{[3]}}\right]$$

$$F_5 = \frac{2b^2 l^3 C_2 \sinh\gamma_2\pi}{\pi^4 \gamma_2^2}\left[-\frac{\kappa_1 \sum_{j=1}^{N_1} b^{[1,j]} E_x^{[1,j]} \varepsilon_1^{[j]}}{E_x^{[1,1]} I_0^{[1]}} - \frac{\sum_{j=1}^{N_1} b^{[1,j]} E_x^{[1,j]} \varepsilon_3^{[j]}}{E_x^{[1,1]} A_0^{[1]} I_0^{[1]}} - \frac{\kappa_2 \sum_{j=1}^{N_3} b^{[3,j]} E_x^{[3,j]} \varepsilon_2^{[j]}}{E_x^{[3,1]} I_0^{[3]}} - \frac{\sum_{j=1}^{N_3} b^{[3,j]} E_x^{[3,j]} \varepsilon_4^{[j]}}{E_x^{[3,1]} A_0^{[3]} I_0^{[3]}}\right]$$

(A3.3-7)

where

$$\varepsilon_1^{[j]} = \frac{\left(\xi^{(j-1)}\right)^3 - \left(\xi^{(j)}\right)^3}{6}$$

$$\varepsilon_2^{[j]} = \frac{\left(\xi^{(j-1)}\right)^3 - \left(\xi^{(j)}\right)^3}{6}$$

$$\varepsilon_3^{[j]} = \frac{\left(\xi^{(j-1)}\right)^2 - \left(\xi^{(j)}\right)^2}{4}$$

$$\varepsilon_4^{[j]} = \frac{\left(\xi^{(j-1)}\right)^2 - \left(\xi^{(j)}\right)^2}{4}$$

$$\varepsilon_5^{[j]} = h^{(j-1)} - h^{(j)}$$

$$\kappa_0 = 2h_0^{[3]} + 2h^{[2]} + 2\xi$$

$$\kappa_1 = h_0^{[1]} - h^{[1]} - \frac{h^{[2]}}{2}$$

$$\kappa_2 = h_0^{[3]} + \frac{h^{[2]}}{2}$$

$$\kappa_3 = \frac{2}{3}\left(h_0^{[1]} - h^{[1]} + \frac{h^{[2]}}{4} \right)$$

$$\kappa_4 = \frac{2}{3}\left(h_0^{[3]} - \frac{h^{[2]}}{4} \right) \qquad \text{(A3.8-17)}$$

In Equations (24)

$$R' = \frac{-l^2\pi^2\left(2G_{1R0}h_1 + 6\alpha'^2 G_{1I0}h_2 + 12G_{2R0}F_1h_3 + 12\gamma_1^2\alpha'^2 G'_{10}F_4h_4 + 12\gamma_2^2\alpha'^2 G'_{20}F_5h_5 - \pi^2 h_6\right)}{12\alpha'\left(\alpha'^4\alpha' S'_2 - l^4 G_{1I0}S'_1\right)h_3}$$

$$h_1 = \alpha'^4\left(F_1 - F_4\gamma_1^2 - F_5\gamma_2^2\right) + \alpha'^2\left[F_1\left(\gamma_1^4 + \gamma_2^4\right) - \alpha\left(F_4\gamma_2^2 + F_5\gamma_1^2\right)\right] + \alpha^2 F_1$$

$$h_2 = \alpha'^4\left(F_3 + F_4 + F_5\right) + \alpha'^2\left[F_3\left(\gamma_1^4 + \gamma_2^4\right) + \left(F_4\gamma_2^4 + F_5\gamma_1^4\right)\right] + \alpha^2 F_3$$

$$h_3 = \alpha'^4 + \alpha'^2\left(\gamma_1^4 + \gamma_2^4\right) + \alpha^2$$

$$h_4 = \alpha'^2 + \gamma_2^4$$

$$h_5 = \alpha'^2 + \gamma_1^4$$

$$h_6 = F_1\left[\alpha'^4 + \alpha'^2\left(\gamma_1^4 + \gamma_2^4\right) + \alpha^2\right]$$

(A3.18-24)

$$G_{1R0} = \frac{\pi\left(\sin 2\pi\eta - \sinh 2\pi\eta\right)}{4\eta\left(\cos 2\pi\eta - \cosh 2\pi\eta\right)}$$

$$G_{1I0} = \frac{\pi\eta\left(\sin 2\pi\eta + \sinh 2\pi\eta\right)}{4\eta^2\left(\cos 2\pi\eta - \cosh 2\pi\eta\right)} + \frac{1}{4\eta^2}$$

$$G_{2R0} = \frac{\pi\left(\sin\pi\eta\cosh\pi\eta - \cos\pi\eta\sinh\pi\eta\right)}{4\eta\left(\cos 2\pi\eta - \cosh 2\pi\eta\right)}$$

$$G'_{10} = \frac{\pi\gamma_1\coth\pi\gamma - 1}{2\gamma_1^2}$$

$$G'_{20} = \frac{\pi\gamma_2\coth\pi\gamma - 1}{2\gamma_2^2} \qquad \text{(A3.25-29)}$$

References

1. Teng JG., Chen JF, Smith ST, Lam L. FRP strengthened RC Structures. Chichester, UK: Wiley, 2001.

2. Cadei JMC, Stratford TJ, Hollaway LC, Duckett WG. C595-Strengthening metallic structures using externally-bonded fibre-reinforced-polymers. London CIRIA, 2004.

3. Swamy RM, Jones R, Bloxham JW. Structural behaviour of reinforced concrete beams strengthened by epoxy-bonded steel plates. The Structural Engineer 1987; 65A(2): 59-68.

4. Triantafillou TC, Plevris N. Strengthening of RC beams with epoxy-bonded fiber-composite materials. Materials and Structures 1992; 25: 201-211.

5. Jones R, Swamy RN, Charif A. Plate separation and anchorage of reinforced concrete beams strengthened by epoxy-bonded steel plates. The Structural Engineer 1988; 66(5): 85-94.

6. Garden HN, Quantrill RJ, Hollaway LC, Thorne AM, Parke GAR. An experimental study of the anchorage length of carbon fiber composite plates used to strengthen reinforced concrete beams. Construction and Building Materials 1998; 12: 203-219.

7. Etman EE, Beeby AW. Experimental program and analytical study of bond stress distributions on a composite plate bonded to a reinforced concrete beam. Cement and Concrete Composites 2000; 22: 281-291.

8. Smith ST, Teng JG. Interfacial stresses in plated beams. Engineering Structures 2001; 23: 857-871.

9. Roberts TM, Haji-Kazemi H. Theoretical study of the behaviour of reinforced concrete beams strengthened by externally bonded steel plates. Proceedings of the Institution of Civil Engineers 1989; Part 2, 87: 39-55.

10. T ä ljsten B. Strengthening of beams by plate bonding. Journal of Materials in Civil Engineering, ASCE 1997; 9(4): 206-212.

11. Malek AM, Saadatmanesh H, Ehsani MR. Prediction of failure load of R/C beams strengthened with FRP plate due to stress concentration at the plate end. ACI Structural Journal 1998; 95 (1): 142-152.

12. Deng J, Lee MMK, Moy SSJ. Stress analysis of steel beams reinforced with a bonded CFRP plate. Composite Structures 2004; 65: 205-215.

13. Stratford T, Cadei J. Elastic analysis of adhesion stresses for the design of a strengthening plate bonded to a beam. Construction and Building Material 2006; 20: 34-45.

14. Tounsi A. Improved theoretical solution for interfacial stresses in concrete beams strengthened with FRP plate. International Journal of solids and Structures 2006; 43: 4154-4174.

15. Tounsi A, Benyoucef S. Interfacial stresses in externally FRP-plated concrete beams. International Journal of Adhesion and Adhesives 2007; 207-215.

16. Qiao P, Chen F. An improved adhesively bonded bi-material beam model for plated beams. Engineering Structures 2008; 30: 1949-1957.

17. Benachour A, Benyoucef S, Tounsi A and Adda bedia EA. Interfacial stress analysis of steel beams reinforced with bonded prestressed FRP plate. Engineering Structures 2008; 30: 3305-3315.

18. Yang J and Wu YF. Interfacial stresses in FRP plated concrete beams: Effect of shear deformation, Composite Structures 2007; 80: 343-351.

19. Tounsi A, Hassaine Daouadji T, Benyoucef S and Adda bedia EA. Interfacial stresses in FRP-plated RC beams: Effect of adherend shear deformation. International Journal of Adhesion and Adhesives 2009; 29: 343-351.

20. Shen HS, Teng JG, Yang J. Interfacial stresses in beams and slabs bonded with thin plate. Journal of Engineering Mechanics ASCE 2001; 127(4): 399-406.

21. Yang J, Teng JG, Chen JF. Interfacial stresses in soffit-plated reinforced concrete beams. Proceedings of the Institution of Civil Engineering, Structures and Buildings 2004; 157: 77-89.

22. Rabinovich O, Frostig Y. Closed-form high-order analysis of RC beams strengthened with FRP strips. Journal of Composites for Construction, ASCE 2000; 4: 65-74.

23. Mukhopadhyaya P, Swamy R N. Interface shear stress: A new criterion for plate debonding. Journal of composites for construction ASCE 2001; 5(1): 35-43.

24. Yang J. The Stress Analysis and Strength Prediction of Plated RC Be*ams*. Ph.D Thesis, School of Civil Engineering, the University of Leeds, UK, 2005.

25. Teng JG, Zhang JW, Smith ST. Interfacial stresses in RC beams bonded with a soffit plate: a finite element study. Constuction and Building Materials 2002; 16(1): 1-14.

26. ABAQUS. ABAQUS/Standard User's Maual. Version 6.3, Hibbitt, Karlsson & Sorensen, Inc , 2002.

27. Gere JM. Mechanics of Materials (5^{th} ed.). Brooks/Cole, USA. 2001.

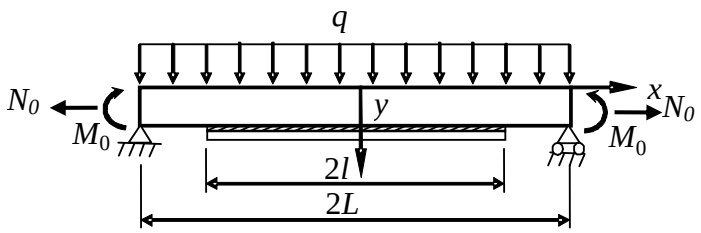

Fig.1 Structural idealisation of the strengthened RC beam

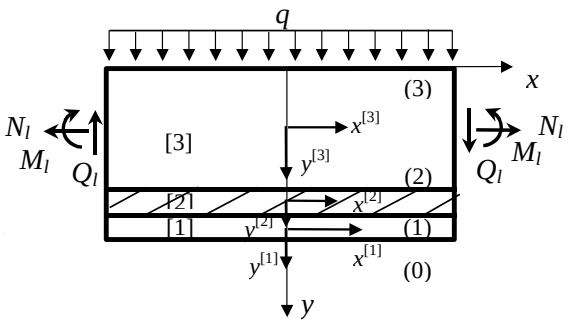

(a) Strengthened beam

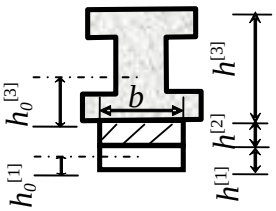

(b) Cross section of the strengthened beam

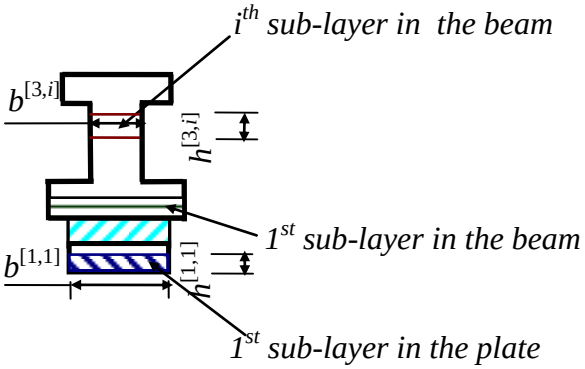

(c) Sub-layers shown in the cross section

Fig. 2 Notations used in the formulation

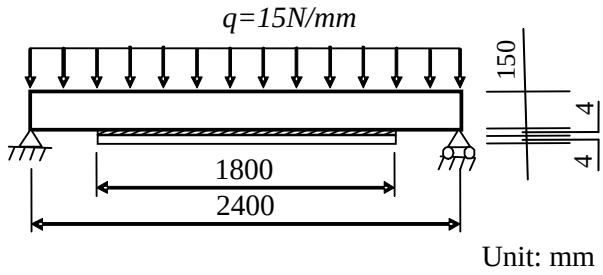

Fig.3 The first example – RC beam bonded with steel plate

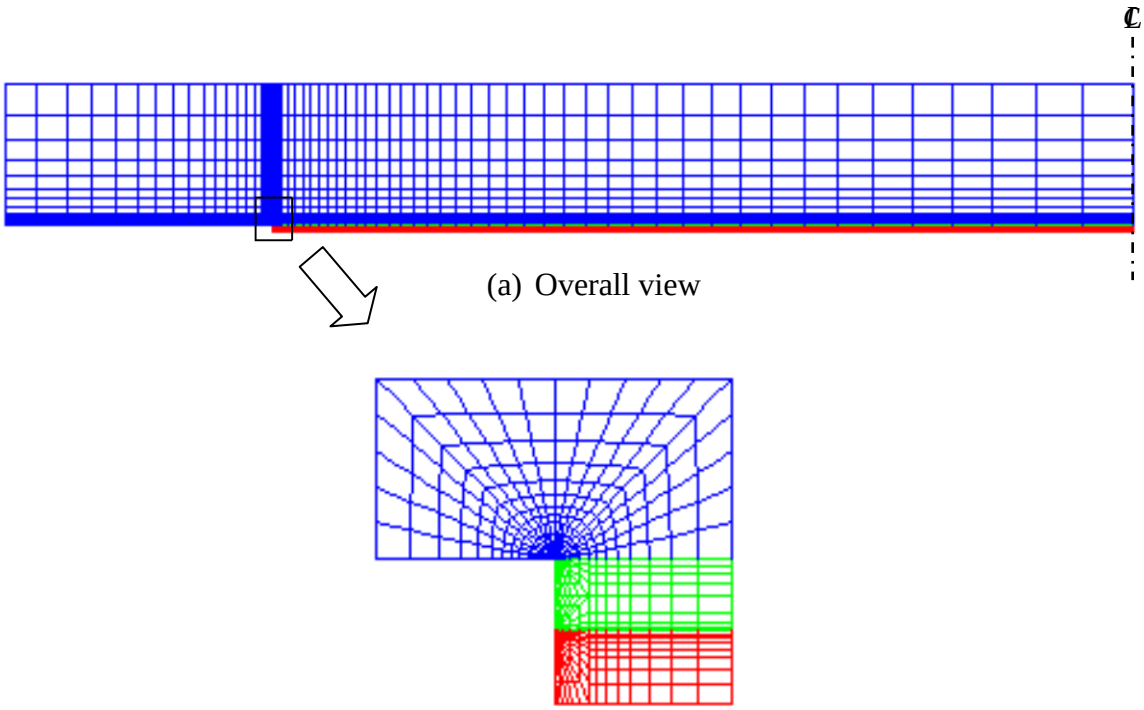

(a) Overall view

(b) Detailed view near the plate end

Fig. 4 Finite element mesh adopted in FEA analysis

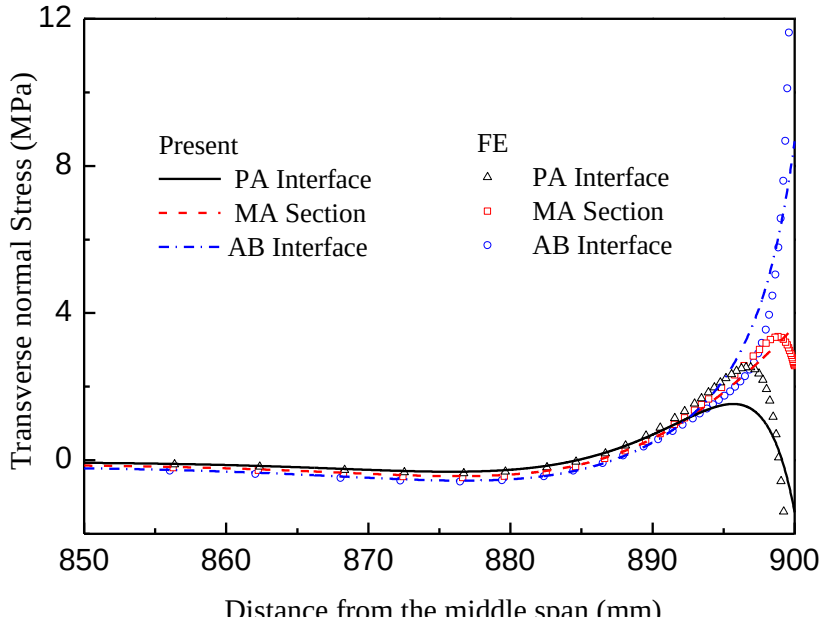

(a) Transverse normal stress

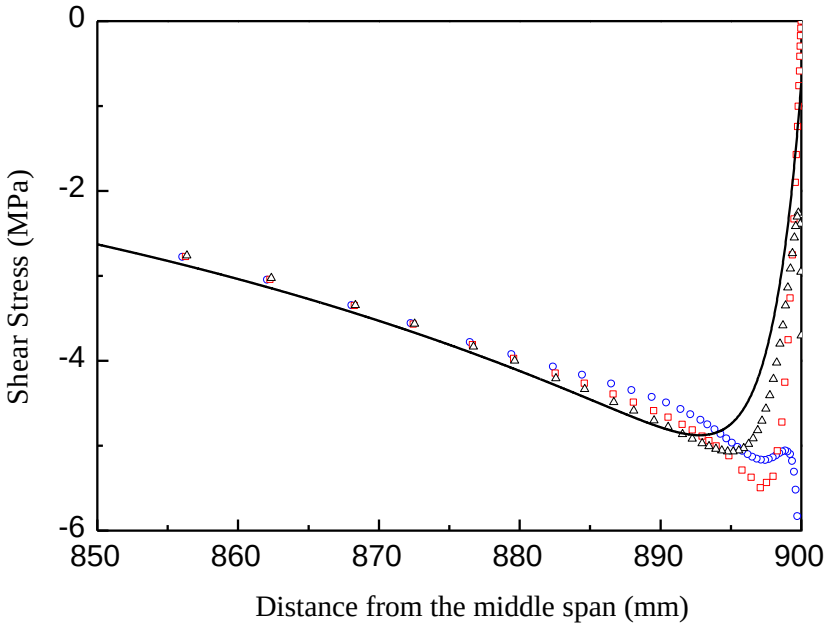

(b) Shear stress

Fig. 5 Steel plated RC beam under UDL

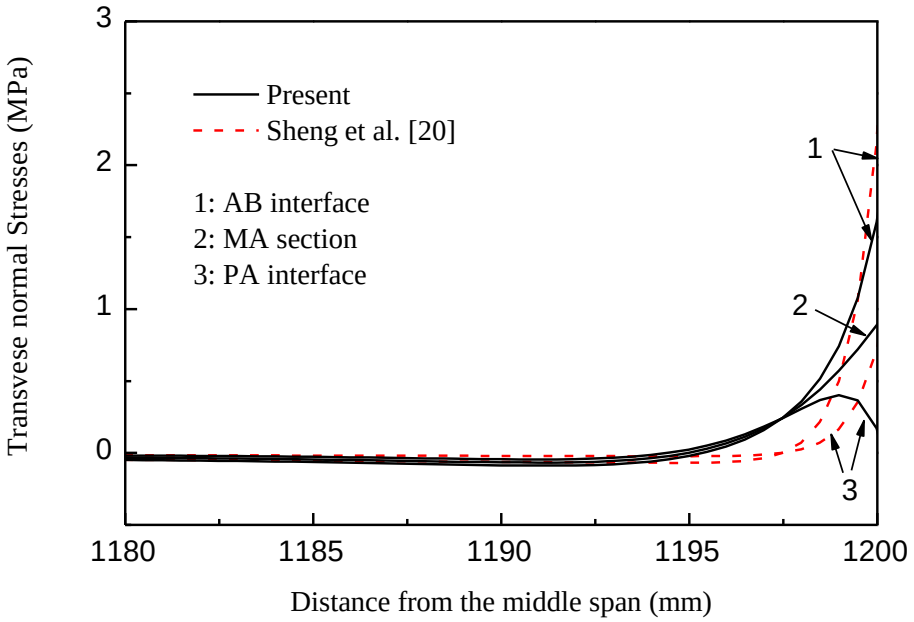

(a) Transverse normal stress

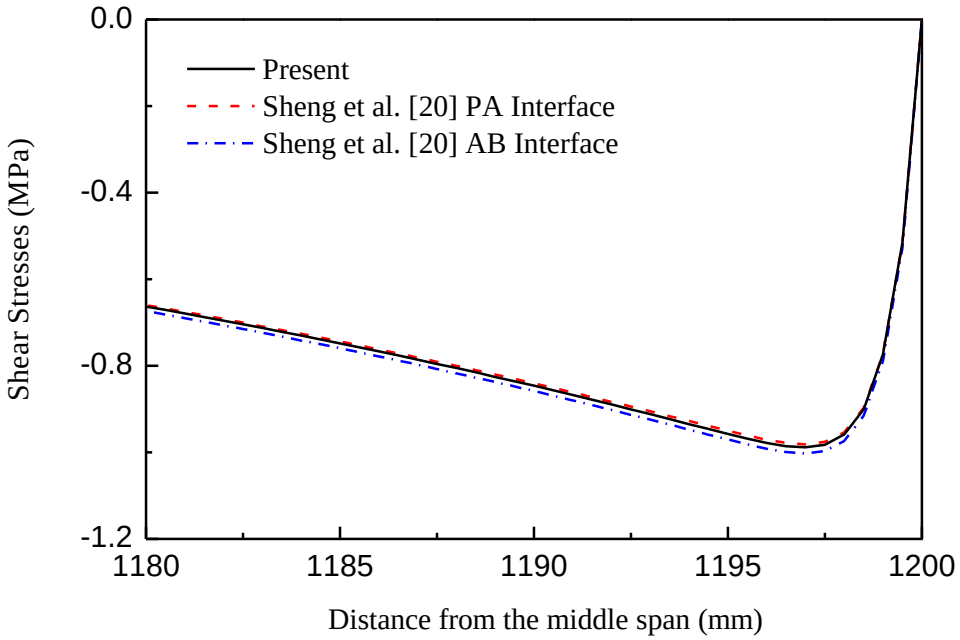

(b) Shear stress

Fig. 6 CFRP plated RC beam under UDL

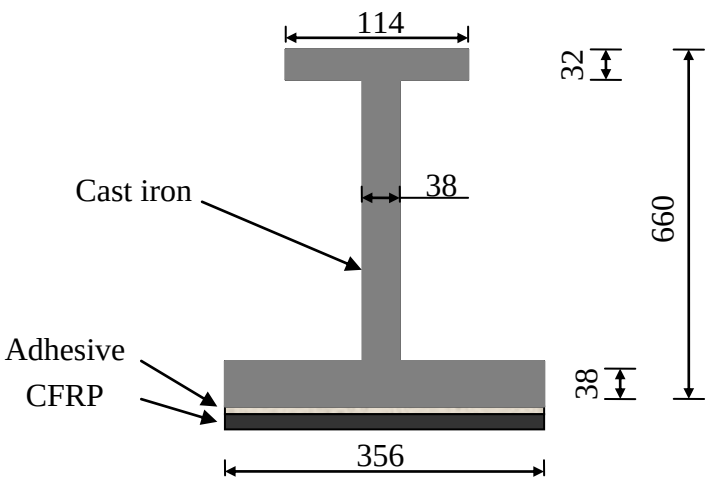

Fig. 7 Cross section of the strengthened cast iron beam

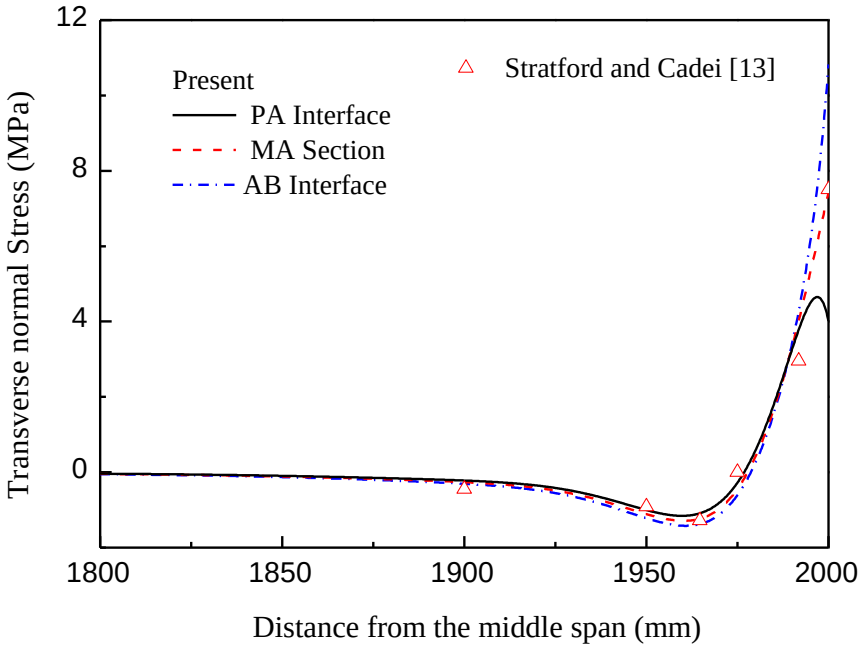

(a) Transverse normal stress

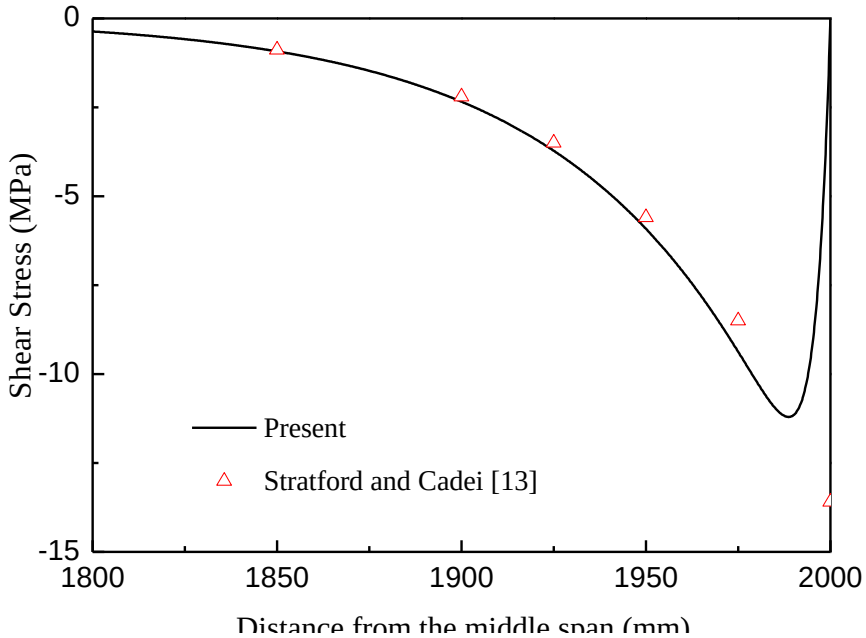

(b) Shear stress

Fig. 8 CFRP plated CI beam under uniform temperature rise

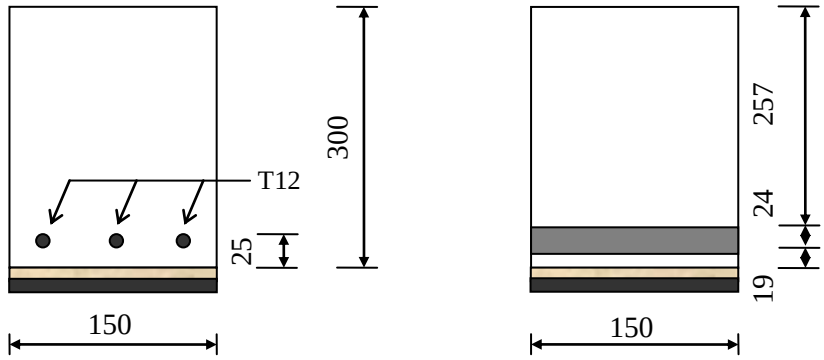

(a) The cross section of the RC beam (b) The equivalent cross section

Fig. 9 Cross sections of the RC beam

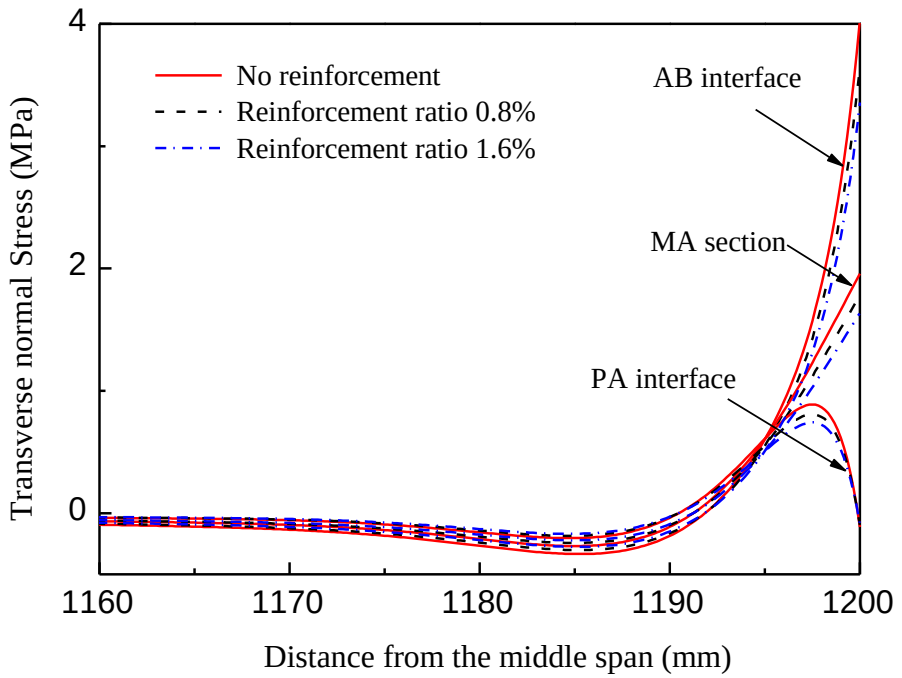

(a) Transverse normal stress

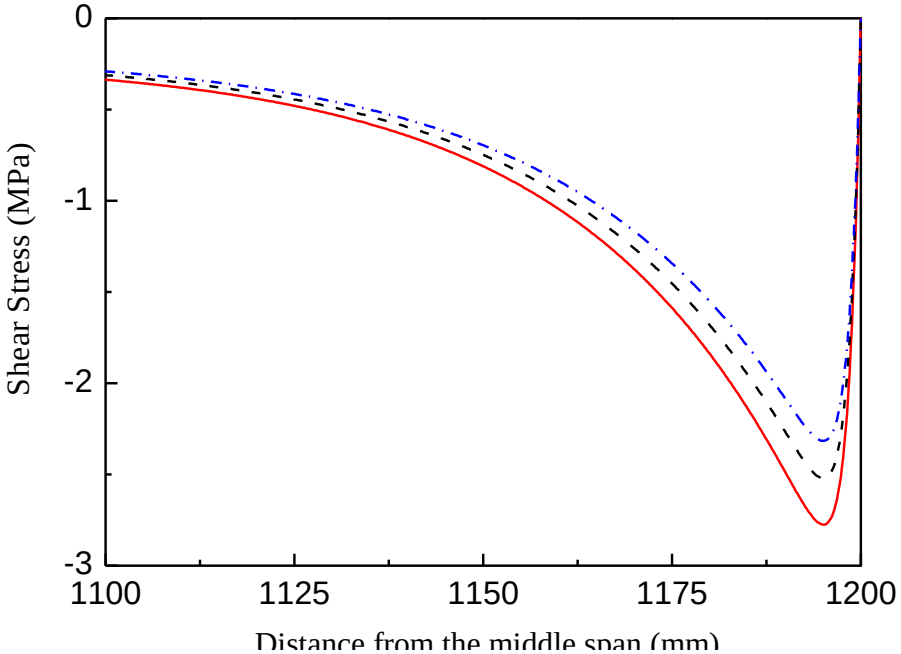

(b) Shear stress

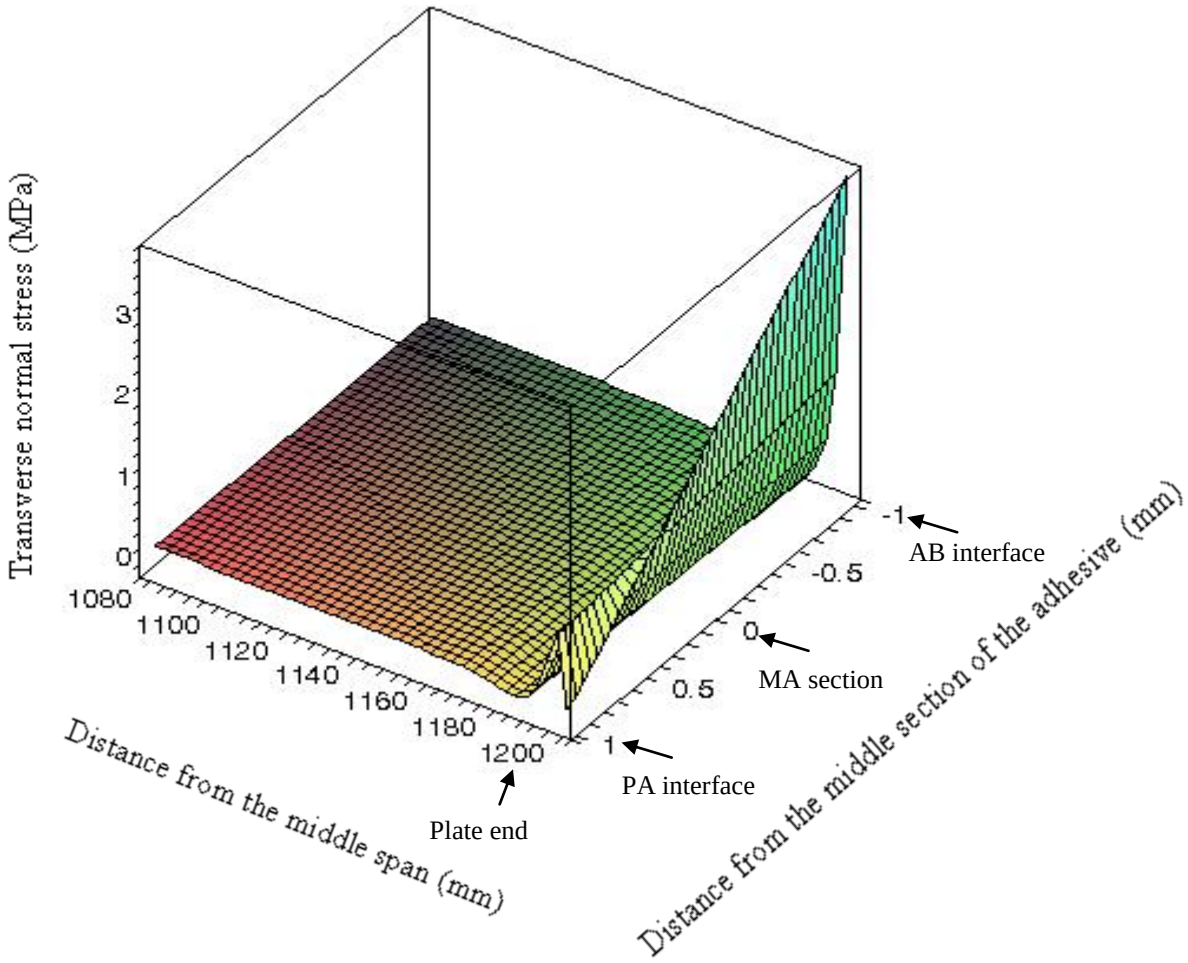

(c) 3-D graph of the transverse normal stress considering the steel reinforcement

Fig. 10 CFRP plated RC beam with and/or without reinforcements